1. INTRODUCTION

In radiotherapy, it is crucial to verify theoretically calculated dose distributions obtained from dose-planning systems by comparing with the real dose distributions from radiation sources. The real dose distribution can be obtained by irradiating a tissue equivalent phantom for which the dose is monitored at certain points spatially distributed in the phantom. For irradiation close to body cavities, verification can also be performed *in vivo* by placing dosimeter probes in the cavities. In these cases, the desired characteristics for a dosimeter are radiation absorption properties similar to those of biological tissues, small size, convenient shape (e.g. small pellets, thin films or gel), the possibility of *in vivo* dosimetry, ruggedness and resistance to environmental conditions. All these requirements are not fulfilled by ionisation chambers or diode detectors. The requirements can be fulfilled by a material which is a dosimeter in itself and thus is independent of electronics for dose registration. Dosimeters of such Radiation-sensitive materials (RSM) are called passive dosimeters. The most common passive dosimeter is the thermoluminescent dosimeter (TLD). One disadvantage with TLD is that the signal is lost during read-out. The signal in electron spin resonance (ESR) dosimeters is however not affected by readout and the dosimeter can thus be read out as many times as needed for improved statistics or dose assessment.

1.1 ESR-DOSIMETRY

ESR-dosimetry is a method of deriving the absorbed dose of an irradiated sample from the ESR-spectroscopy signal of that sample, where the signal is proportional to the magnetic moment of stable radiation induced radicals which are propotional to the absorbed dose. ESR-spectroscopy is one of the most important analytical methods in a vast number of fields of chemistry and biophysics. For dosimetry purposes ESR is used in industry and medicine as well as in geological and archaeological dating. Important medical applications are dose assessment for sterilization and catastrophe medicine (Mc Laughlin 1993) as well as radiotherapy (Bartolotta et al 1993). Promising results for use in quality control of x-rays have also been made (Malinen et al 2004). The possibility of *in vivo* ESR (Gallez & Swartz 2004, Regulla 2005) and imaging (Lurie 2001) has been reviewed and promising results in respective area (Schauer et al 2007, Deng et al 2004) has recently been achieved.

1.2 THE ALANINE DOSIMETER

Crystalline L-α-alanine has been used as an ESR-dosimeter material since the 1960:s (Bradshaw et al 1962). Among its favourable properties are the linear dose response which holds up to 10 kGy (Regulla & Deffner 1982) and even higher if correction for heating is performed (Nagy et al 2000b), the chemical composition which makes alanine nearly tissue equivalent (Olsson et al 2002b) and the radical stability which allows reproducible readouts a year after irradiation if the dosimeter is stored in normal laboratory conditions (Sleptchonok et al 2000). Alanine dosimeters are commercial available in different shapes and has long been a standard for transfer dosimetry between national laboratories world wide (Mc Laughlin 1993). An international standard for alanine dosimetry has been accepted (ISO/ASTM 2004). The uncertainties for alanine dosimeters irradiated at radiotherapy dose levels of 1-5 Gy have been shown to be 1.5-4% (Nagy et al 2002). For dose levels of 5-50 Gy uncertainties below 0.5% have been achieved (Anton 2005). Thus, at radiotherapy dose level, alanine dosimeters have been tested and used as a promising alternative to TLD by the laboratories of NIM in Peoples Republic of China (Juncheng & Zaiyong 1996) and IAEA (Mehta & Girzikowsky 1996). For brachytherapy alanine has been used for radiation source calibration in water phantom (Angelis 1999) and in agarose gel (Olsson et al 2002b) and *in vivo* measurement (Schaeken & Scalliet 1996) in shape of thin film. Alanine dosimeters have also been used as a promising alternative to TLD for calibration of the irradiation source in transfusion therapy (Fainstein et al 2000)

1.3 IMPROVED ESR-DOSIMETRY TECHNIQUES

Although acceptable uncertainties have been achieved for dose levels of the order of Gy the sensitivity need to be further improved to achieve higher spatial resolution and better precision at sub-gray levels to be of use for radiotherapy dose distributions of quality control or *in vivo* measurements. The potential for even further reduction of the uncertainties at lower dose levels are however far from being exhausted (Nagy 2000a).

Spectrometers that are dedicated for dosimetry has been developed (Maier & Schmalbein 1993). Uncertainties due to uncontrollable variations of spectrometer sensitivity have been successfully reduced by use of reference samples (Nagy et al

2000c). Alanine dosimeters incorporating a reference material, which can be used for self-calibration and correction of instrumental errors, have been produced (Yordanov & Gancheva 2002) although a recent international intercomparison showed large uncertainties due to non-standardised calibration methods (Gancheva et al 2007).

The precision has been further improved by spectral processing (Ruckerbauer et al 1996, Hayes et al 2000, Anton 2005) and advanced signal quantification algorithms (Sharpe et al 1996, Castro et al 2006) have been successfully implemented. More accurate numerical treatment of calibration has also been suggested (Bergstrand et al 1998, Nagy 2000a).

1.4 NEW DOSIMETER MATERIALS

Although alanine has become a state of the art passive dosimeter, the pursuit for higher dosimetric sensitivity also involves investigations of alternative materials. Strategies for finding such materials have been purposed (Ikeya et al 2000). Apart from enhanced radical yield, properties of importance for improved sensitivity include spectral shape and influence of readout parameters (Lund et al 2002).

Organic materials such as 2-methylalanine (Olsson et al 2002b) and perdeuterated alanine (Gancheva et al 2006) have twofold higher signal intensities than alanine. Among other organic materials of interest are ammonium tartrate which also is twice as sensitive as alanine (Olsson et al 1999) and can be made even more sensitive by deuteration (Olsson et al 2000).

Organic materials have the advantage over TLD of being tissue equivalent but on the other hand the spectra are often broad and complicated due to hyperfine structure. This effect can be reduced by metal ions in metal salts of organic acids (Ikeya et al 2000). The ionic bonding will also increase the band gap, and intentional doping with aliovalent cations, as is commonly done for TLD, might enhance the sensitivity (Hassan & Ikeya 2002). Several of these materials seem to be promising, such as lithium lactate (Hassan et al 1998) lithium acetate dihydrate and lithium phosphate (Hassan & Ikeya et al 2000) as well as Li-citrate and Li-oxalate (Hassan & Ikeya 2002). Potassium ditionate

has been shown to be 10 times as sensitive as alanine (Lund et al 2002). The intensity has also been increased twofold by isotope enrichment (Lund et al 2004) and doping with metal chlorides (Lund et al 2005).

In year 2000 the author of this review performed an experimental investigation of six salts of formic- and lactic acids proposed and provided by Professor Anders Lund of the University of Linköping. The salts of formic acid were composed of a formate anion while cations respectively were lithium, sodium and potassium. The salts of lactic acid were composed of a lactate anion while cations were lithium, calcium and zinc, respectively. Lithium formate, calcium lactate and zinc lactate are bound to crystal water. As a reference alanine was also analysed. Crystalline alanine is in itself both anion and cation.

Table 1 Analysed substances with chemical structure formula and abbreviation used in this report.

Substance	Chemical structure formula	Abbreviation
Lithium formate monohydrate	$HCOO^- Li^+ * H_2O$	LiFo
Sodium formate	$HCOO^- Na^+$	NaFo
Potassium formate	$HCOO^- K^+$	KFo
Lithium lactate	$CH_3CH(OH)COO^- Li^+$	LiLa
Calcium lactate tetrahydrate	$(CH_3CH(OH)COO^-)_2 Ca^{2+} * 4H_2O$	CaLa
Zinc lactate trihydrate	$(CH_3CH(OH)COO^-)_2 Zn^{2+} * 3H_2O$	ZnLa
L-α-Alanine	$CH_3CH(NH_3^+) COO^-$	Ala

Lithium formate was found to be a good candidate and has been subjected to several studies (Lund et al 2002, Vestad et al 2003, Lund et al 2004, Malinen et al 2004, Vestad et al 2004a, Vestad et al 2004b, Lund et al 2005) during the last years. However, no report of the study in the year of 2000 was ever produced. Although the results of that study are now dated they can be of use as an example of this review.

1.5 AIM OF THE REVIEW

This is a review of the technique of ESR-dosimetry and strategies for investigation of new materials as in regard to their applicability as ESR-dosimeters for radiotherapy. The applicability of the dosimeter is judged by evaluating the tissue equivalence, radical yield, radical stability, spectral suitability, optimal readout parameters, dose response and sensitivity of the dosimetric system. The materials and experimental data of the study in the year of 2000 are used as an example of the investigation.

2. REVIEW OF ESR DOSIMETRY: THEORY AND METHODS

A dosimeter is a detector of ionising radiation for which the detector reading, M, is the product of the detector efficiency, η, the mean absorbed dose of the detector material, $\bar{D}_{det}$, and the mass of the material, m_{det} (Alm-Carlsson 1981b).

$$M = \eta \bar{D}_{det} m_{det} \quad (1)$$

The detector efficiency is determined by a physical change produced by the radiation in the material and the instrumental quantification of this change. In ESR dosimetry the physical change is radiation induced radicals. Radicals are defined as atomic or molecular species with unpaired valence electrons (Lewis 1916). Thus, the physical quantity is density of unpaired electrons, N_V, which is measured by means of ESR spectroscopy (Bradshaw et al 1962).

Direct measurement of N_V requires knowledge of experimental parameters which are difficult to obtain and it is therefore a common practise to use a reference sample with N_V obtained by other techniques of chemistry (Regulla & Deffner 1982).

In principle an absolute dose determination is possible based on knowledge of the radical yield and the number of radicals induced by ionizing radiation but due to experimental difficulties the overall uncertainty of such absolute concentration measurements can be as high as 50%. Hence ESR dosimetry is commonly used as relative method based on calibration against a standard of dosimetry, such as an ionisation chamber (Regulla & Deffner 1982). In such a calibration the relative dose response is obtained in arbitrary units of spectrometer reading (Bradshaw et al 1962). The calibration factor, N_D obtained can be used for dose assessment following the equation (Regulla & Deffner 1982, Bartolotta et al 1993)

$$D = N_D \left(l - l_0\right) \prod_i k_i \quad (2)$$

Here l is the detector reading normalised to dosimeter mass and l_0 is the normalised reading at zero dose (Bergstrand et al 1998). For dose assessment were the conditions of measurement are in variance with those of the calibration, correction factors k_i have to

be applied. They include correction factors for influence parameters of irradiation, readout and environmental effects (De Angelis et al 1999).

Evaluation of new dosimeter materials requires detailed knowledge of the influence parameters and for this purpose the theoretical background and experimental methods of ESR dosimetry are reviewed here.

2.1 ABSORBED DOSE OF THE DOSIMETER

One of the most important issues of dosimetry is precise definition of the quantity to be measured. The equation of detector reading (Eq1) is based on the mean absorbed dose of the detector material but this quantity is neither of primary interest nor straightforward to obtain through calibration towards a detector of another material. Thus, the dosimetric system is calibrated to the quantity of interest which for radiotherapy is dose to water, D_w. The relation between the two quantities might depend on the irradiation conditions and quality. Furthermore, in ESR dosimetry it is important to distinguish between the radiation sensitive material, $\bar{D}_{RSM}$, and any binding material of the dosimeter in which it is incorporated. The mean dose of the dosimeter sample, $\bar{D}_s$, and $\bar{D}_{RSM}$ might not be the same and their relation is dependent on the dosimeter geometry and radiation quality. For conversion between dose of the detector and a medium of interest a modifying factor, $f = \bar{D}_{det} / D_m$, need to be determined (Alm-Carlsson 1981b).

2.1.1. Radiation interaction

The modifying factor, *f*, is independent on physical means of dose measurement and is thus only dependent on the radiation interaction of the detector and medium (Alm-Carlsson 1981b). In theory the absorbed dose can be calculated according to a general equation (Alm-Carlsson 1981a), neglecting spontaneous nuclear transformations

$$D = \sum_j \int \frac{d\Phi_j(T)}{dT} \frac{\mu_j(T)}{\rho} \overline{\Delta\varepsilon_j}(T)\, dT \qquad (3)$$

as a product of the fluence Φ_j of ionising particles of type j , their total interaction cross section per unit mass μ_j/ρ and the average of energy imparted $\Delta\varepsilon_j$ for the interactions.

The practical difficulty of direct calculation of the dose in this manner, due to lack of detailed information about distributions and basic processes, can often be overcome by assumptions of various kinds of radiation equilibria explained below.

In a medium irradiated with indirectly ionising particles for which the mean free paths are considerably longer than the ranges of the charged particles they liberate, charged-particle equilibrium (CPE) can be assumed. Similarly, for a medium irradiated with charged particles, δ-particle equilibrium (DPE) can be achieved if the ranges of the primary particles are longer than those of the liberated δ-particles. For media irradiated with electrons or high energy photons the approximation of partial δ-particle equilibrium (PDPE) can be used if the ranges of δ-particles with energy less than a specified value Δ are considerably shorter.

If CPE is assumed, the dose can be calculated with knowledge of the energy fluence of uncharged particles Ψ and the mass energy-absorption coefficient μ_{en}/ρ. For DPE or PDPE the dose is correspondingly obtained by the fluence of charged particles Φ and the mass collision stopping power coefficient S_{coll}/ρ. Because of the energy dependence of these coefficients it is convenient to use the mean energy coefficients.

$$\frac{\overline{\mu}_{en}}{\rho} = \frac{\int_0^{E_{\max}} \frac{\mu_{en}}{\rho} \frac{\psi}{dE} dE}{\int_0^{E_{\max}} \frac{\psi}{dE} dE} \tag{4}$$

$$\frac{\overline{S}}{\rho} = \frac{\int_\Delta^{T_{\max}} \frac{S_{coll}}{\rho} \frac{d\Phi}{dT} dT}{\int_\Delta^{T_{\max}} \frac{d\Phi}{dT} dT} \tag{5}$$

where Eq5 is the mean restricted stopping power.

The validity of radiation equilibrium is thus ultimately defined by the range of charged particles and for photon or electron irradiated media in particular, by electron range.

2.1.2. Electron range

The range of electrons or δ-electrons needs to be compared to mean free path of primary particles for equilibrium as well as the depth in the material for build up. Furthermore it

defines which density of an inhomogeneous medium to be used for calculations of the mean chord length g [g/cm^2] of radiation tracks across the dosimeter volume and the correction due to the density effect of stopping power. For example pellets of crystal powder which can be used as ESR dosimeters (Bradshaw et al 1962) typically have a diameter of a few millimetres and are composed of crystal grains of sub millimetre size, interspaced by binding material or void. Hence, for both the detector volume and inhomogeneities in the material the size compared to electron range is essential.

In the cavity theory of Burlin (1966) the effective mass absorption coefficient for electrons β [cm^2/g] is used as an indirect measure of the electron range compared to g. To account for the energy distribution of electrons in a photon irradiated medium Burlin approximated β by a formula introduced by Loevinger (1956) for β–rays in air.

$$\beta = 16.0\left(E_m - 0.036\right)^{1.40} \tag{6}$$

Solid state detectors are often of intermediate size compared to electron range (Burlin 1966) and thus $\beta \cdot g$ is close to unity. This would certainly be the case for a an ESR-dosimeter with a diameter of a few millimetres in a MV-photon field but compared to inhomogeneities in the detectors sub millimetre size the electron range would be long.

2.1.3. Cavity theory

In cavity theories the dosimeter sample is viewed as a cavity in the surrounding medium and the dose relation between the cavity and the medium can be calculated with the modifying factor f.

$$\bar{D}_c = f \cdot D_m \tag{7}$$

If, for a cavity in a photon irradiated medium, CPE can be assumed, the dose gradients of the interfaces be neglected and the electron range is considerably shorter than g, then, the dose to the cavity can be calculated using the ratio of mass energy-absorption coefficients.

$$f = \left(\bar{\mu}_{en}/\rho\right)_m^c = \frac{\left(\bar{\mu}_{en}/\rho\right)_c}{\left(\bar{\mu}_{en}/\rho\right)_m} \tag{8}$$

If the electron range is longer than the mean cord length and the electron fluence is the same in the medium and the detector, the dose can be calculated according to the cavity

theory of Gray (1935) or Spencer and Attix (1955) assuming DPE or PDPE respectively and using the mean restricted stopping power in the latter case.

$$f = {}_m\bar{s}_m^c = \frac{\bar{S}_c/\rho}{\bar{S}_m/\rho} \tag{9}$$

As mentioned in the preceding section solid state detectors are often of intermediate size compared to electron range of radiotherapy energies. In such cases *f* can be modelled according to the cavity theory of Burlin (1966).

$$f = d \cdot {}_m\bar{s}_m^c + (1-d)\left(\bar{\mu}_{en}/\rho\right)_m^c \tag{10}$$

The dimensionless factor *d* is a weighting factor depending on the size of the cavity and the range of electrons.

$$d = \left(1-e^{-\beta g}\right)(\beta g)^{-1} \tag{11}$$

The cavity theory of Burlin is semi empirical and only valid for small difference in atomic composition of the cavity and surrounding medium. Rigorous analytical parameters have been successfully developed but their applicability is limited to simplified one-dimensional analysis whereas a general cavity theory has to be Monte Carlo based (Frujinoiu 2001).

Cavity theories require particle equilibria. Furthermore they do only account for the mean dose to the cavity. Bergstrand et al states that not even Monte Carlo would account for any microdosimetric effects or chemical yield variations due to the crystals suspended in binder material in a crystal powder ESR-dosimeter. Presumably this is a consequence of inadequate models due to lack of knowledge in this particular situation.

2.1.4. Tissue equivalence

For calibration or absolute dosimetry measurements the irradiation situation is well known and accurate dose calculations according to the preceding section can usually be performed. In most situations of relative dosimetry and *in vivo* dosimetry the details of the radiation field might not be known. Therefore it is preferable if the dosimeter is as close as possible to water or the tissue of interest.

Sufficient but not inevitably necessary conditions of tissue equivalence are likeness in atomic composition as well as isotopic abundance (for neutrons). For specific irradiation

conditions differences in atomic compositions are acceptable if the resultant deviations in mean mass energy-absorption and mean stopping power quotients cancel each other which might be the case for low-atomic-number media with coefficients which are numerically very close. This is one cause to the relative successfulness of the cavity theory of Burlin (Frujinoiu 2001). Nevertheless, even small discrepancies result in interface effects and other perturbations of the radiation field. Hence, experimental verification of tissue equivalence is of fundamental importance.

The absorbed dose to Ala is very close to that to water for direct irradiation with ^{60}Co or MV-photon fields but Ala receives somewhat less dose in β-radiation and proton fields whereas the dose to Ala in kV-photon fields is only 2/3 to that of water (Bradshaw et al 1962, Regulla & Deffner 1982). Films of Ala, calibrated in a ^{60}Co-field, has been shown to agree with measurements with ionisation-chamber and Monte Carlo simulations of dose distributions due to both 6 and 15 MV photon fields in homogenous phantom and various phantoms with interface layers (Østerås et al 2006). LiFo provides precise dose measurements with low dependence on the electron energy (6–20 MeV) for dosimetry of clinical electron beams (Malinen et al 2007).

Sometimes substantial deviations in tissue equivalence can be of advantage because of relatively higher signal and the possibility to discriminate different types of radiation. For example enrichment of the ^{6}Li isotope in LiFo dramatically increases the capture cross-section for thermal neutrons for which the relative dose contribution is of radiation biological interest (Lund et al 2004). The dose to LiFo compared to that of the less tissue equivalent calcium formate has proved to be useful for determination of radiation quality of kV x-rays (Malinen et al 2004).

2.1.5. Calibration of ESR dosimeters

A batch of dosimeters i can be calibrated by irradiating them with a range of doses D_i determined through a traceable standard for the dose quantity which is sought for. If the dose response is linear the readout of the dosimeters l_i can be fitted by linear regression to a function of D_i, a determinable zero dose signal l_0 and individual fluctuations ε_i.

$$l_i = aD_i + l_0 + \varepsilon_i \tag{12}$$

The constant "a" is the slope of the regression curve and the inverse of the calibration constant N_D (Bergstrand et al 1998).

As mentioned in the previous sections, this type of calibration is relative to the spectrometer characteristics and settings. Thus, all relevant conditions of the calibration must be stated (ISO/ASTM, 2004) and used for calculation of correction factors k_i when N_D is employed for dose assessment.

2.2 QUANTITATIVE ESR SPECTROSCOPY

Although ESR-dosimetry (being used as relative method) neglects the absolute value of N_V, awareness of the relation between this quantity and the spectrometer reading is still important for issues of proper instrumentation, spectral quantification, and the influence parameters of the readout. Thus, the paramagnetic behaviour of radical samples and their instrumental quantification through resonance spectroscopy is briefly reviewed.

Despite the numerous advanced methods of ESR spectroscopy developed during the last six decades, the basic method of Continuous Wave (CW) ESR is still the standard for quantification of radicals or other paramagnetic species. In a CW ESR spectrometer (fig2) the sample to be analysed is continuously irradiated with electromagnetic radiation of a fixed frequency. A strong magnetizing field is applied so that the magnetic flux density B in the sample is varied to find values, B_r, at which the sample is in resonance with the applied electromagnetic field. The following presentation is limited to the present case of CW ESR spectrometer operating at the microwave x-band with a reflection resonant cavity and magnetic field modulation. This is one of the most common configurations and most results are also valid for other configurations.

2.2.1. Paramagnetic interaction of unpaired electrons

Orbital electrons preferably group in pairs (Lewis 1916) with different sign of half unity value of the spin quantum number m_s of which the sum cancels (Pauli 1925). However, unpaired electrons exhibit spin magnetic dipole moment which magnetises the close surroundings thus giving rise to a total magnetic dipole moment, μ, which in a crystal

lattice is called paramagnetic centre. The strength of μ is given by the Bohr magneton μ_B and the electron spin g-factor which depends on local magnetisation.

$$\mu = -g\mu_B m_s \tag{13}$$

Depending on the positive or negative sign of m_s the direction of μ is parallel or anti-parallel to an applied magnetic field B and the population densities of the corresponding states of paramagnetic centres are commonly denoted N_α and N_β, respectively. Each state is characterised by the potential energy of the dipole moments (fig1) in the applied field, $U=-\mu B$, and the transition energy between the states is given by (Rabi 1937):

$$\Delta E = U_\alpha - U_\beta = g\mu_B B \tag{14}$$

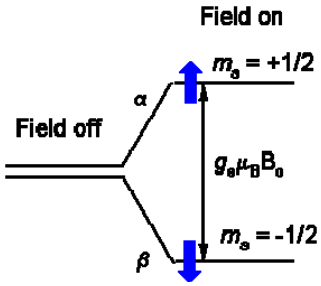

Fig1 Paramagnetic states of an unpaired electron and their energy.

Electrons in a magnetic field precess (Larmor 1897) with the Larmor frequency $\nu_0 = g\mu_B B/h$ (Rabi 1937) which equals the resonance frequency of the microwave radiation (Bagguley et al 1948). At resonance a net absorption of radiation is observed (Zeeman 1897, Lodge 1897) as a result of the difference between absorption and stimulated emission of the radiation corresponding to the difference in population density (Purcell et al 1946).

$$\Delta N_V = \left(N_\beta - N_\alpha\right) \tag{15}$$

For thermal equilibrium at the absolute temperature T, ΔN_V is given by the state distribution according to Boltzmann statistics $N_\alpha / N_\beta = e^{-\Delta E / k_b T}$, where k_b is the Boltzmann constant and the assumption $\Delta E \ll k_b T$ (Bloembergen et al 1948).

$$\Delta N_V = \frac{\Delta E}{2k_b T} N_V \tag{16}$$

Hence at room temperature in a common ESR 0.3T field the states are almost equally populated, ($\Delta N_V \approx 10^{-3} N_V$). By recognising that the macroscopic magnetisation is the sum

of the magnetic dipole moments, $M = \mu \cdot \Delta N_V$, it becomes evident that the sample is paramagnetic and follows the curie-formula for paramagnetic susceptibility (Bloch 1946) with the vacuum permeability μ_0:

$$\chi_0 = \frac{\mu_0 M}{B} = \frac{N_V \left(g \mu_B\right)^2}{4 k_b T} \tag{17}$$

2.2.2. ESR resonance absorption

The energy absorption rate of the microwaves at frequency v_1, due to the effective magnetic field component B_1 over the sample, is proportional to the imaginary part of the complex dynamic susceptibility χ'' (Portis 1953, Gallay & Van Der Klink 1987) which is a function of v_1, the static susceptibility χ_0 and the probability density for absorption as a function of magnetic flux density $\rho(\Delta B)$ (Bloembergen et al 1948)

$$\chi'' = \frac{\pi}{2} v_1 \chi_0 \gamma^{-1} \rho\left(\Delta B\right) \tag{18}$$

where $\gamma = g \mu_B / \hbar$ [s^{-1} T^{-1}] is the gyro magnetic ratio and $\Delta B = B - B_r$ is the magnetic field offset by the resonance value.

A group of paramagnetic centres with the same B_r is henceforth denoted spin packet. According to Eq16, 17 and 18 the absorption rate is proportional to the population difference ΔN_V. The change of ΔN_V is balanced by interaction with the crystal field (Bagguley et al 1948) through absorption and stimulated emission of quantized lattice vibrations, called phonons, which can change the spin state of paramagnetic centres. Hence the magnetisation fades to its equilibrium value with the spin-lattice relaxation time T_1 (Bloch, 1946). Similarly, the interaction between the magnetic dipoles equilibrates local magnetization of specific spin packets (Bagguley et al 1948) after the spin-spin relaxation time T_2 (Bloch 1946) but is on the other hand of no consequence for the gross magnetization. Incorporating these interactions yields the probability distribution of absorption line shape for a single spin packet (Bloch, 1946)

$$\rho\left(\Delta B\right) = \frac{1}{B_1^2 \gamma^2 T_1 T_2 \cdot \left(1 + \Delta B^2 \gamma^2 T_2^2\right)^{-1} + 1} \cdot \frac{\gamma T_2}{1 + \Delta B^2 \gamma^2 T_2^2} \tag{19}$$

The first factor is called saturation factor (Bloembergen et al 1948) and will be considered below while the second factor is a Lorentzian line shape with the half width at half maximum $\Gamma = \left(\gamma T_2\right)^{-1}$. Hence a sample with strong spin-spin dipole interaction due to short mean distance between dipoles will have a broader absorption line shape (Bagguley et al 1948). This is of dosimetric interest for high LET radiation. For instance, dipolar broadening between CO_2^- radicals trapped in the tracks of α-particles has been attributed as the physical cause of the increase in line width occurring after neutron irradiation in comparison with photon irradiation of the ^{6}Li doped LiFo sample (Lund et al 2004, Malinen et al 2006).

If B_1 is small enough the saturation factor will be close to unity but as B_1 increases the equilibrium value of ΔN_V is no longer maintained by the relaxation and thus the net absorption decreases (Bloembergen et al 1948). This is illuminated by expressing the radiation field in terms of incident power $P=B_1^2/c^2$ by the conversion factor c and introducing $P_0=(c^2\gamma^2T_1T_2)^{-1}$ (Sagstuen et al 2000), called the spin relaxation parameter (Malinen et al 2006). At resonance, the saturation factor of Eq19 becomes $(P/P_0+1)^{-1}$ and thus P need to be far less than P_0 to avoid saturation. P_0 can be experimentally obtained by saturation measurements (Sagstuen et al 1997a) and can be used for calculation of relaxation times if c is known.

2.2.3. The ESR-spectrometer

In an ESR-spectrometer (fig2) the sample is contained in a cavity where it is scanned by an electromagnet by stepping through a preset range of B. Through a waveguide the cavity is connected to a microwave source and a detector, to which it reflects the radiation.

The incident power P on the cavity is regulated by an attenuator in the waveguide. The connection between the waveguide and the cavity is controlled by an adjustable opening called the iris. By adjusting the phase and frequency of the microwaves as well as the iris, the microwaves can be brought to resonance in the cavity and will form standing waves (fig3a) with a maximum of B_1 and a minimum of the corresponding electric field component E_1 at the sample (fig3b). If the iris is properly tuned no microwaves will be

reflected from the cavity but will dissipate as ohmic losses of currents in the cavity walls. The ratio between the energy of the microwaves stored as standing waves in the cavity and the lost microwave power is called the quality factor, Q (Portis 1953).

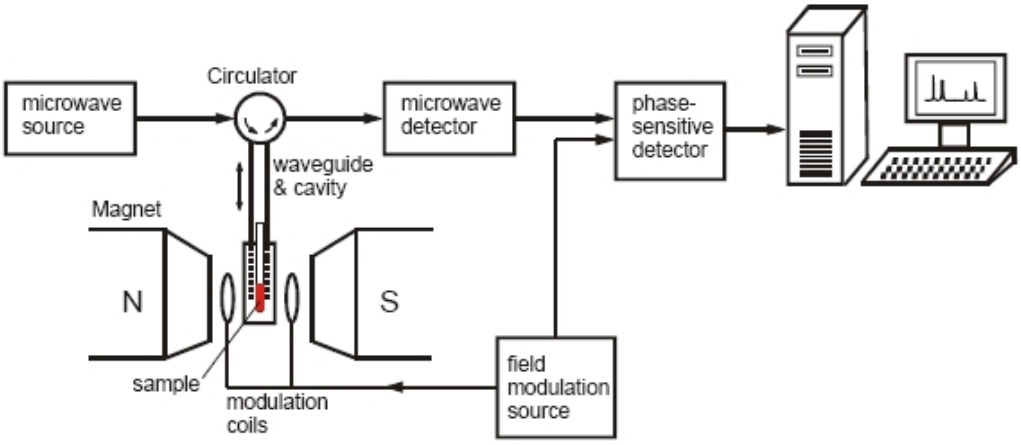

Fig 2 Schematic block diagram of the ESR-CW spectrometer (From Jeschke 2003)

The fraction of B_1 at the sample compared to the entire cavity is called filling factor η and is proportional to the fraction of the sample volume and the volume of the cavity (Goldberg & Crowe 1977). The relation between the B_1 and the applied power P depends on the values of Q and η (Gallay & Van Der Klink 1986) and thus, according to the previous sub section, so does P_0. The position, shape and dielectric properties of the sample are critical factors for Q and η. Thus, efforts of optimising sample shape have recently been performed (Yordanov et al 2006).

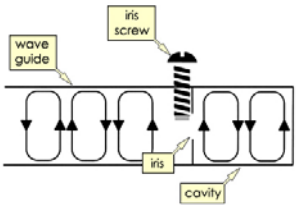

Fig3a The iris of the waveguide is adjusted to achieve standing waves in the cavity and no reflection back to the waveguide. (From Bruker BioSpin 1999)

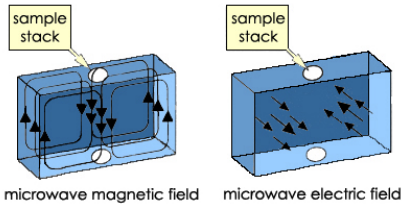

Fig3b The magnetic and electric field due to standing waves in the cavity. The stack for the sample test tube is indicated (From Bruker BioSpin 1999)

If the microwaves are brought to resonance with the sample the absorption of microwaves will bring the cavity out of resonance and thus the stored microwaves will be reflected out of the cavity. The reflected microwaves will be absorbed by the detector producing an electric signal V proportional to the square root of the reflected power P_r

for which the relation to the applied power has been derived for CW ESR (Gallay & Van Der Klink 1987).

$$V = K \cdot \sqrt{P_r} = K \cdot Q\eta\chi'' \cdot \sqrt{P} \qquad (20)$$

The proportionality is dependent on detector parameters which are not easily obtained (Regulla & Deffner 1982) and is therefore conveniently summarised by a constant K (Maruani 1972).

In most ESR-spectrometers a sinusoidal, time dependent magnetic field, called modulation field, is superimposed to B (fig4a). The main purpose of this is to discriminate disturbing signals from the signal reflected from the cavity but the technique also improves signal processing.

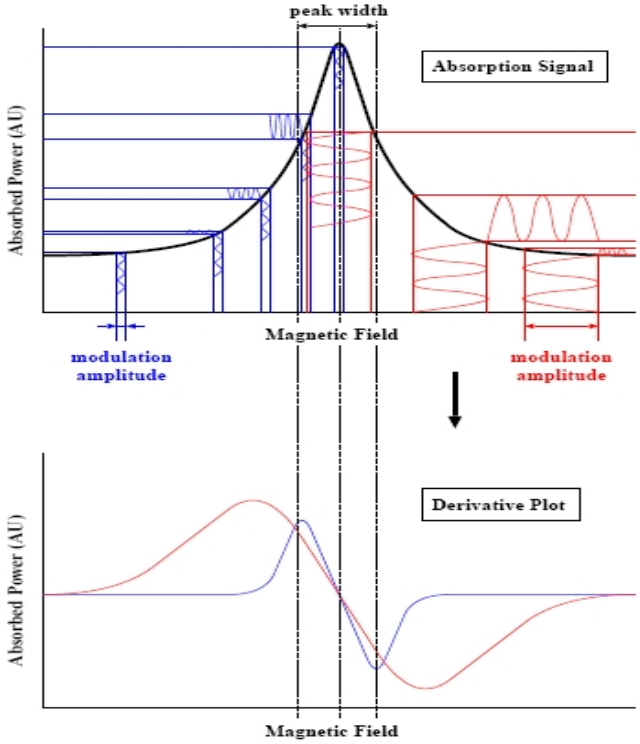

Fig4a Moderate modulation (left in upper part), overmodulation (right in upper part) and the resulting output spectra (lower part). (From Truitt 2004)

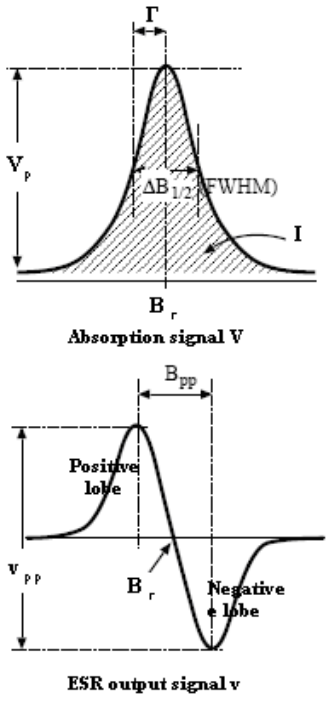

Fig4b Principal shape of spectral peaks and abbreviations used to describe spectral characteristics. (After Truitt 2004)

The modulation has the frequency, ν_m and modulation amplitude, B_m (Bloembergen et al 1948). The reflected microwave field will have the shape of superimposed harmonics (Wahlquist 1961) of the modulation frequency (fig4a, upper part). Normally the first harmonic is extracted by a phase sensitive detector (fig2) which acts as band pass filter

of modulation frequency. The amplitude of this signal will be the ESR output signal (Wahlquist 1961). For low values of B_m the ESR output signal is approximately the derivative of the absorption signal (fig4b) with respect to the magnetic flux density (Bloembergen et al 1948) and the intensity is proportional to B_m (Wahlquist 1961).

$$v(B) = \frac{dV}{dB} \cdot B_m \tag{21}$$

For modulation amplitude in the order of the width of the non-modulated peak λ_{pp} the absorption derivative approximation is not valid. Instead the measured peak width B_{pp} and peak height v_{pp} are distorted (fig4a).

The detector and all the other spectrometer devices are interconnected by electronic circuits regulating the spectrometer settings and transferring measurement data to a computer system. The modulated ESR-signal is electronically amplified and filtered with preset Receiver gain (*RG*) and time constant of the filter but only the latter parameter improves *S/N*. The analogue output is digitised by sampling the signal integrated during the conversion time (t_c) and the result is stored in the computer as floating point numbers y^x in a string of a preset number n_{ch} of data points x (channels) corresponding to discrete steps of the *B*-field scanning. Increasing the conversion time also improves *S/N* but makes the recording time longer. Furthermore the time constant of the filter is limited by t_c to avoid distortion.

To further reduce noise the spectrum can be re-scanned any number of times (n_{scan}) and the result is added in the computer for each data point. The signals from each spectrum will add linearly while (normally distributed) noise will only increase with the square root and hence *S/N* will increase with the square root of n_{scan}.

2.3 QUANTIFICATION OF ABSORBED DOSE

The spectrometer output is a spectrum of data points. From this a single valued quantity need to be extracted as input quantity of the measurand absorbed dose. This procedure requires detailed knowledge of the spectral characteristics and their dependence of dose, readout parameters and influence quantities.

2.3.1. ESR Spectrum

Realistic ESR spectra are composed of line shapes from several spin packets due to physical interactions, as reviewed below. This has impact on both the spectral characteristics and the dependence of readout parameters.

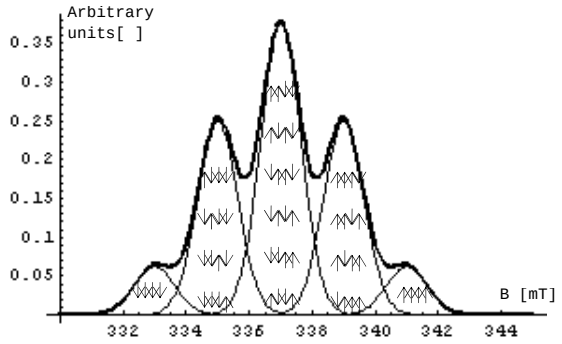

Fig5a Interaction with four nuclear magnetic moments (like for Ala) producing five absorption peaks with indicated degeneracy.

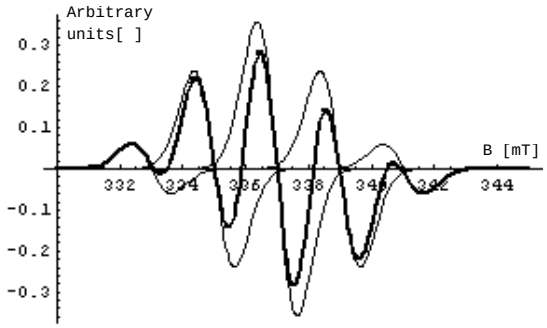

Fig5a Derivative spectrum (first harmonic output) of the absorption peaks to the left..

Nuclear magnetic dipoles are important in ESR-spectroscopy because of their so called hyperfine splitting (hfs) interaction with electron magnetic dipoles (Bleaney et al 1949). The transition energy (14) is thus slightly modified by the nuclear magnetic dipoles.

$$\Delta E = g\mu_B B + \sum A_0 m_I \qquad (22)$$

were A_0 [J] is the hyperfine coupling constant and m_I is the nuclear spin quantum number for which the probability of transition is negligible during electron spin resonance. Hence, resonance will occur at several different field strengths. The intensity will depend on the degeneracy of Eq22 for each resonance energy (fig5a and b). If the hfs constant is in the order of the full width at half maximum (2Γ) of the peaks, then the super positioned peaks will not be readily resolved.

Both the g-factor and the hyper fine constant A_0 might be anisotropic with regard to the crystal orientation compared to the direction of the magnetic field. In a single crystal sample this will resulting variations in resonance frequency with crystal orientation (Bleaney et al 1949) but in a powder sample of randomly oriented crystals it will result in asymmetric broadening of the resonance peaks. The broadening effect can be cancelled by deconvolution of the spectrum (Ureña-Nuñez et al 1993).

According to Eq19 a spin packet is more saturated at lower values of P at the centre of the line than at the side lobes. This is important when spin packets of different B_r overlap. Such a superposition of line shapes is called inhomogeneous broadening and can be caused by hyperfine interaction, anisotropy broadening, dipolar interaction between different spin packets and inhomogeneities in applied field (Portis 1953). This is modelled by the convolution of Eq19 with an envelope function which is normally taken to be of Gaussian distribution. The result is a much broader spectral peak with the shape of a Voigt distribution (Maruani 1972). The theory has been refined to include degrees of inhomogeneous broadening (Castner 1959) and singularities (Maruani 1972). The saturation behaviour can be modelled by

$$V \propto \sqrt{P}\left(P/P_0 + 1\right)^{-\alpha} \tag{23}$$

with $1>\alpha>0.5$ corresponding to extreme cases of homogenous and inhomogeneous broadening (Sagstuen et al 1997a).

If B_m is not negligible compared to λ_{pp}, Eq21 does not hold. The spectral shape is distorted from the derivative of the absorption signal, the observed peak width B_{pp} increases and the increase of v_{pp} becomes slower than the linear dependence of B_m. At high values of B_m the increase of B_{pp} becomes a linear function of B_m and v_{pp} decreases. The relations have been solved analytically for Lorentzian shape function in parameter form (Wahlquist 1961) and in explicit form (Arndt 1965). For Gaussian distributions it can not be solved analytically but a numerical solution has been obtained (Smith 1964) and the numerical data for v_{pp} and B_{pp} is presented in fig 6a and b.

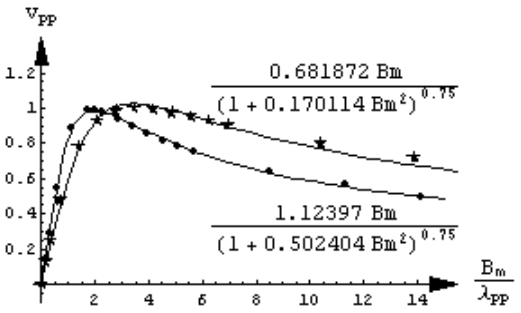

Fig6a Fitting of model function for v_{pp} to the data of Wahlquist (stars, upper expression) and Smith (dots, lower expression).

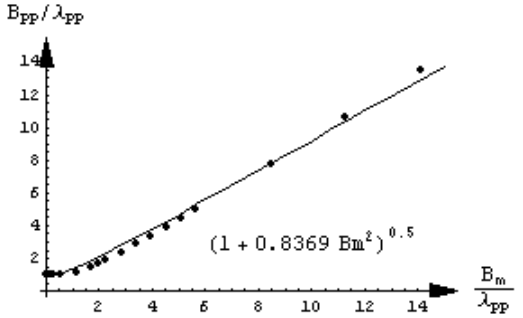

Fig6b Fitting of model function for B_{pp} to the data of Smith.

It is useful to apply semi-empirical model for analysis of experimental data. The square of the Gaussian line width has been shown to be equal to the square of λ_{pp} plus the square of B_m times a constant (Bales et al 1998). Using the fact that B_{pp} of a Voigt line shape is approximately equal to the Gaussian line width when the latter is much broader than the Lorentzian line width (Olivero & Longbothum 1977), it is evident that B_{pp} can be modelled by (24a). Based on this conclusion and the equations of Arndt (1965), a similar equation (24b) is herby proposed for v_{pp}.

$$B_{pp}^2 = \lambda_{pp}^2 + \kappa^2 B_m^2 \tag{24a}$$

$$v_{pp} = K \cdot B_m \left(\lambda_{pp}^2 + \kappa^2 B_m^2 \right)^{-3/4} \tag{24b}$$

If $\omega_m T_1$ is not small enough for each spin packet to be completely relaxed the saturation behaviour is altered by the modulation (Bloembergen et al 1948, Portis 1953). The displacement of the saturation curve maximum has been derived as a function of B_m/λ_{pp} (Brotikovskii et al 1973). The fact that P and B_m are not independent variables has been noted for 2-methylalanine (Olsson et al 2002a) and systematically examined for alanine, lithium formate, magnesium formate and calcium formate (Vestad et al 2003).

2.3.2. The spectrometer signal

The output of the spectrometer is a string of floating point numbers y corresponding to the channels x. Each y^x is composed of a reproducible and a non-reproducible part

$$y^x = v^x + \partial v^x \tag{25}$$

The non-reproducible signal ∂v^x consists of non-linear background and high frequency noise (Ruckerbauer et al 1996). The reproducible part v^x is composed of the Radiation induced signal (RIS) and Background signal (BGS) which might include unknown previously received dose or non-radiation induced background signals (Ivannikov et al 2002).

Although BGS has been demonstrated to dominate the spectrum for unirradiated Ala there are also contributions from the microwave cavity and the sample holder (Wieser et al 1993), henceforth denoted Spectrometer background signal (SBG).

Based on these facts the composite signal v can be viewed as a function of dosimeter mass m, dose D and constants a corresponding RIS, BGS and SBG respectively for each data point x.

$$v^x = a^x_{RIS} \cdot m \cdot D + a^x_{BGS} \cdot m + a^x_{SBG} \tag{26}$$

For a spectrum of known shape of RIS but unknown intensity and BGS contribution, the signals can be separated by least square regression of the first two terms of Eq26 (Ciesielski et al 2007).

2.3.3. The spectrometer reading

For dosimetric purposes a single quantity representing the absorbed dose need to be extracted from the spectrum. Such quantities are (fig4b) the peak-to-peak height of the output spectrum v_{pp}, the height of the absorption peak V_p and the integral of the absorption peak I (Lyons 1997). Minimizing interference is the most important issue although data processing and robustness with noisy spectra must also be taken into account (Lyons 1997). The uncertainty of dose calibration has been shown to be less for Ala when v_{pp} is used as the output quantity instead of I (Ahlers & Schneider 1991). For Ala the linearity of v_{pp} as a function of I has been verified (Malinen et al 2003a).

The spectral quantity of interest is a question of what it is needed for and how accurate the extraction from the spectrum is. Thus the integral of the absorption I is needed for concentration measurements whereas the other quantities are sufficient for all other purposes. Compared to v_{pp}, V_{p} is less sensitive to high frequency noise but much more sensitive to baseline distortion and peaks are more difficult to detect and resolve (Lyons & Tan 2000). Thus, except for the concentration measurement, v_{pp} is commonly chosen as the quantity to represent absorbed dose, as has become standard practice for Alanine dosimeters (ISO/ASTM, 2004).

At high modulation amplitude v_{pp} reaches a local maximum whereas V_{p} approaches a limit asymptotically and I increases linearly. The latter cases do however not offer any advantage because the increase is merely due to line broadening (Arndt 1965) and the signal will thus be excessively prone to systematic errors due to baseline deviation and finite integration limits (Lyons & Tan 2000).

Derivation of the output spectrum would decrease the contribution of broad baseline deviations, although it would increase the high frequency noise. The latter might not be the case if the second harmonic was recorded in the first case. In fact, for Ala, the second harmonic signal has been shown both to reduce baseline deviation and improve *S/N* (Chen et al 2002). The technique also increased the optimal modulation amplitude although the relative signal increase due to modulation was less (Chen et al 2002) which is in accordance with the theory for the modulated Lorentzian (Arndt 1965).

2.3.4. Normalisation to a spin concentration reference

Samples with unpaired electrons in d- and f-orbitals (e.g. Mn^{2+} or Fe^{3+}) are often used as reference standards for N_V in ESR-dosimetry. The influence of variations in spectrometer parameters can be cancelled by normalisation of the spectrometer reading of the sample to that of a spin concentration reference samples. Correction for *P* or *Q*-factor variation is sufficient if both the sample and the reference are in the linear region of the microwave power dependence (Nagy et al 2000c). The same holds for modulation amplitude. The technique does not correct for time dependent inhomogeneities of the fields in the cavity.

2.4 RADICAL YIELD

The sensitivity of the ESR-dosimetry system is a product of the spectroscopic sensitivity and the number density of radicals, N_V , per unit absorbed dose of the sample, D_s [Gy]. This section deals with the latter quantity in terms of production of radicals (radiolysis), their characteristics, their disappearance (radical recombination) and the dependence on influence parameters as well as their influence on the sensitivity due to different spectrometer parameters.

2.4.1. Radiation yield of radicals

Radiation chemical yield *G* can be defined as the number of induced radicals *N* of a given species per unit absorbed dose and per unit mass *m* [kg] of the sample.

$$N = GmD \tag{27}$$

m refers to the mass of the radiation sensitive material and thus the mass of a binder material must be excluded. For Ala, the radical yield has been confirmed to be

dependent on radiation energy and LET (Bradshaw et al 1962) as well as the irradiation temperature (Nagy et al 2000b). The latter dependence is corrected by a temperature coefficient (ISO/ASTM, 2004). However the yield appears to be independent of dose rate (Regulla & Deffner 1982).

Doping metal-ion organic salts with Ni and Rh have been shown to increase the signal and investigations indicate that these impurities take part in primary electron capture processes, promoting the increased radical yield (Lund et al 2005). At equal and moderate settings of microwave power and modulation amplitude, LiFo doped with $NiCl_2$ was almost four times more sensitive compared to Ala (Danilczuk et al 2007). The signal of Ni and Rh doped samples was about 3–4 times that of the pure lithium dithionate and more than 10 times stronger than the Ala signal. These impurities also shortened T_1 (Gustafsson et al 2005).

If the relative yield of different radicals is altered this can lead to variation of spectrum shape. Although this does not affect I, it can result in significant variations of v_{pp} (Regulla & Deffner 1982). The power saturation behaviour of Ala has been shown to differ for different radicals (Malinen et al 2003a) but for Ala irradiated with 6–19 MeV electrons and 10 kV–15 MV photons at a dose of 10 Gy, the relative amounts of radicals are virtually independent of the beam quality (Malinen et al 2003b). Variations in shape have also been observed for LiFo when irradiated with fast neutrons compared to photons (Malinen et al 2006). The spectral changes due to doping metal-ion organic salts with Ni and Rh are not significant (Gustafsson et al 2005, Danilczuk et al 2007).

2.4.2. Linearity of the dose response

For Ala the dose response of ESR dosimeters has been established to be linear (Bradshaw et al 1962, Regulla & Deffner 1982) in the dose region for radiotherapy. The radical yield saturates at very high doses due to irradiation induced destruction of radicals (Snipes & Horan 1967). Although Ala saturates above 10 kGy the net radical production continues up to the MGy region (Regulla & Deffner 1982). The temperature coefficient of Ala has also been shown to be dose dependent at high doses (Nagy et al 2000b).

A small dose-dependence of the peak-to-peak ratio recently detected in the 4-24 Gy region of LiFo was probably caused by small background signal, originating in the EPR cavity or sample support system, (Malinen et al 2006)

When the density of radicals and thus χ'' become large enough the absorption in the sample will degrade the *Q*-factor of the cavity (Goldberg & Crowe 1977). Furthermore the shorter mean distance between spin dipoles will reduce T_2. In accordance with the theory presented in the previous sections both these effects will increase P_0 and such behaviour has in fact been observed for Ala at high doses (Wieser & Girzikowsky 1996).

2.4.3. Radiation products

The dominant radical of irradiated Ala is called SAR (Stable Alanine Radical). Recent studies have shown that there are two other radicals (fig7) that contribute to the spectrum (Sagstuen et al 1997b). The radicals have been found to contribute to the composite spectrum in the approximate proportions 55-35-10 (Heydari et al 2002).

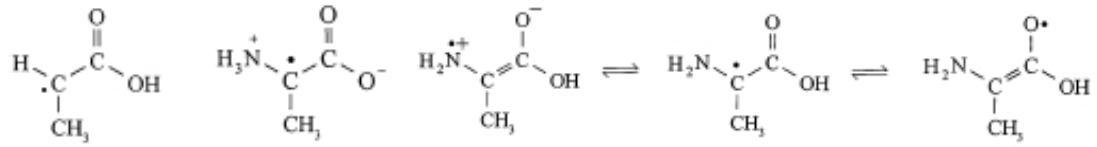

Fig7 From left too right: The SAR radical, the Ala R2 radical and the Ala R3 radical with the radical spin density at different atoms indicated as three different configurations. (After Sagstuen et al 1997b).

A spectrum with several contributing radicals could imply a dosimetric problem because the relative contribution to the spectrum might depend differently on readout parameters and environmental factors for each radical (Malinen et al 2003a, Malinen et al 2003b, Dolo & Moignau 2005b).

For irradiated formates the dominant radical has been reported to be $\dot{C}OO^-$ although for LiFo the existence of another, yet unidentified, radical has been proposed (Vestad et al 2004a). $\dot{C}OO^-$ will keep the ionic bonding to the cation (fig8a) because of the negative charge. The spectroscopic impact of the crystal structure (fig8b) for LiFo has been previously evaluated (Vestad et al 2004a). For LiLa the radical has been reported to be CH_3-$\dot{C}$(OH)COO-Li^+ (Hassan & Ikeya et al 2000).

$$HCO_2^-Li^+ \xrightarrow{h\nu} HCO_2Li^+ + e^-$$
$$HCO_2Li^+ \rightarrow \cdot CO_2^-Li^+ + H^+$$

Fig8a Radical formation in LiFo. (AfterVestad et al 2004a)

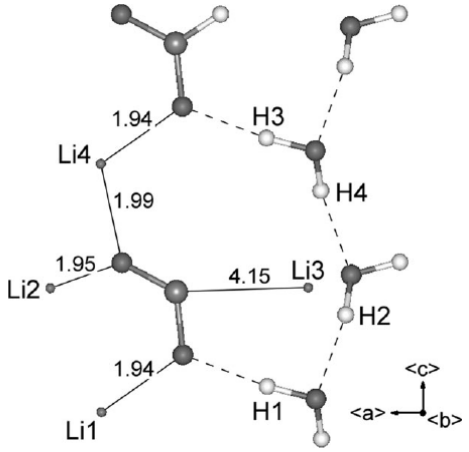

Fig8b Crystal structure around a radical in LiFo (After Vestad et al 2004a)

2.4.4. Radical stability

Although crystals are static in a macroscopic sense, each crystal basis is in constant motion constrained by the columbic forces of the lattice. There is a probability for diffusing of a point defect to lattice sites where the radicals are consumed by chemical reactions which thereby lowers N_V. For irradiated Ala and other organic radicals the mechanisms for this have been shown to be of first order kinetics and thus the decay is exponential (Horan et al 1968). The macroscopic term for radical decay is fading which actually refers to the fading in the recorded ESR-signal of measurements repeated over time. If I is not used as spectrometer reading, fading will also be affected by time dependent variations of spectrometer sensitivity and changes in the spectrum not dependent on N_V.

Just after radiation a fast fading of short lived radicals can occur. This has previously been observed for ammonium tartrate (Olsson et al 1999) and for Ala as a result of different environmental conditions (Dolo & Feaugas 2005a).

For Ala the radical kinematics of different radicals are correlated so that the fading of one radical leads to increase that of another (Heydari et al 2002, Dolo & Moignau 2005b).

The fading characteristics vary with different radical products and environmental conditions such as temperature, humidity and light exposure (Regulla & Deffner 1982). Humidity affects water content for Ala even when incorporated in pellets with hygrophobic binder materials (Arber & Sharpe 1993). The fading of Ala as a function of both temperature and humidity, before and after irradiation, has recently been thoroughly analysed by Dolo & Feaugas (2005a). The effect of humidity has been identified as reversible diffusion of water (free water) and irreversible reactions with water (bound water) changing the radical content through radiolysis and radical recombination (Dolo & Feaugas 2005a).

Radical transformations due to humidity have been demonstrated to change the spectral shape (Dolo & Moignau 2005b). High modulation amplitude can cause heating which changes the water content during readout (Sleptchonok et al 2000). This affects both the radical stability and the Q-factor and thus the total signal fading is an overestimate of the radical recombination.

Although the decrease of I of Ala due to exposure of light has been shown to be moderate, the v_{pp} of the central peak has been shown to decrease significantly due to transformations of radicals (Regulla & Deffner 1982, Ciesielski et al 2004). UV-light has also been found to increase the background signal of Ala (Wieser et al 1993).

3. MATERIALS AND METHOD

3.1 DOSIMETER MATERIAL

All substances of the study (table 1) were provided in powder form. Although all substances are commercially available in powder form some of them had been prepared by Professor Anders Lund in the laboratory of chemical physics at the Linköping University.

3.1.1. Preparation of samples

The powder was pressed, by means of a table-top pellet press, to pellets of cylindrical shape with a diameter of 4.7 mm and a height of 2-3 mm. As described in sub section 2.1.2 the measured dosimeter densities are not the same as the crystal densities found in chemical tables (table 2).

Table 2 Analysed substances and their densities. KFo was found to be hygroscopic and thus the measurement of sample density is not applicable (NA) for this substance. For crystal density of the salts of lactic acids no information was found (NIF).

Substance	Sample density [g/cm^3]	Crystal density [g/cm^3]
LiFo	1.1	1.46
NaFo	1.4	1.92
KFo	NA	1.91
LiLa	1,0	NIF
CaLa	1,0	NIF
ZnLa	1,4	NIF
Ala	1.1	1.42

3.1.2. Handling and storage

All dosimeters were prepared, irradiated and readout in normal but uncontrolled room temperature, pressure and humidity. Samples were stored in transparent plastic boxes that were exposed to both electric light and sunlight from the windows. The storage boxes were not tight fitted and thus the samples were in direct contact with the surrounding air. The time between radiation and readout was 12-24 hours. For the test of radical stability the sample was stored inside the resonance cavity for three months.

3.2 IRRADIATION

The irradiation was performed at the department of radiotherapy, Linköping university hospital. A 4 MV, Varian Clinac 600, accelerator was used. The 4 MV accelerator is a common modality for external radiotherapy and thus it is a natural choice for evaluating dosimeter materials for clinical use. In some measurements, however, availability as well as fast and easy use of an x-ray radiation equipment was preferable to the clinical radiation quality and patient-simulating set-up.

3.2.1. Accelerator irradiation setup

The irradiation setup followed the standard calibration procedure at the radiotherapy unit (fig9). A PMMA-phantom was placed at the source-surface distance (SSD) of 100 cm with the incident field to the phantom set to 10*10 cm^2. A stack of samples was placed in a PMMA cylinder which was inserted at the reference depth for calibration in the phantom. An ionization chamber was inserted as a dose monitor reference from the opposite side but at the same depth.

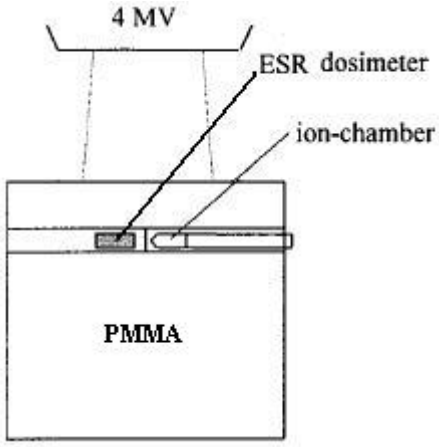

Fig9 Experimental set-up during clinical irradiation of pellets (After Olsson & Bergstrand 2001).

3.2.2. Radiation doses

For most substances two pellets were irradiated at each dose, using 30, 60 and 100 Gy. For lithium formate five pellets were used to obtain better statistics and more dose levels were used to test the dose linearity more accurately. Following the calibration strategy outlined by Nagy (2000a) most calibration points were chosen in the low dose region. Thus, in addition to the former dose levels 1, 2, 5, 10, 15 and 80 Gy was used.

3.2.3. Accelerator dose monitoring

The actual doses obtained were monitored with an NE 2571 ionisation chamber at the reference depth in the phantom. A Janus electrometer was used. The ionisation chamber and electrometer were calibrated to dose to water and the calibration was traceable to a Primary standard dosimetry laboratory. The combined uncertainty of the NE 2571 dosimetric system was 2%.

3.2.4. Absorbed dose calculations

Although the quantity of interest in radiation therapy is dose to water calibration of ESR-dosimeters to this quantity can not be taken to be generally valid. In view of the fact that the energy dependence of the mass energy-absorption coefficients and stopping power are not the same for the different materials the applicability of the calibration routine is limited to the radiation quality for which the calibration was performed. If energy dependence of radiation yield and spectral shape can be neglected the absorbed dose in the ESR-dosimeter material itself is thus a more applicable measure of the dosimeter sensitivity. Hence, dose calculation of the dosimeter material was performed according to Eq7 and 10.

The uncertainty of absorbed dose of the dosimeter as calculated from the monitored dose to water according to the cavity theory of Burlin (1966) is $\delta D_s = \sqrt{\left(D_w\right)^2 \left(\delta f_i\right)^2 + f^2 \left(\delta D_w\right)^2}$. The uncertainty of f is difficult to estimate and thus the overestimation (Olsson et al 2002b) that the uncertainty is the rectangular distribution, over the entire range of f due to variation of d from 0 to 1, was chosen: $\delta f = \sqrt{\left(f_{d=1} - f_{d=0}\right)^2 / 12}$.

3.2.5. Radiation quality of the accelerator

For calculations of tissue equivalence and the modifying factor of cavity theory the photon energy fluence (fig10a) and the electron fluence (fig10b) spectra at the reference point in the phantom need to be established. Data was taken from a Monte Carlo simulation made by Jonas Söderberg and reported by Olsson and Bergstrand (2001).

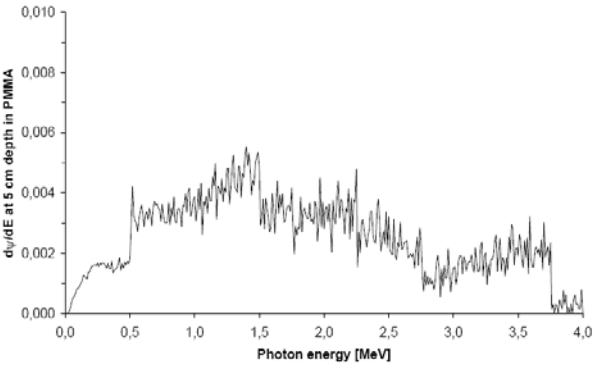

Fig10a Photon energy fluence at the reference depth in the phantom irradiated with 4MV photons. (After Olsson & Bergstrand 2001).

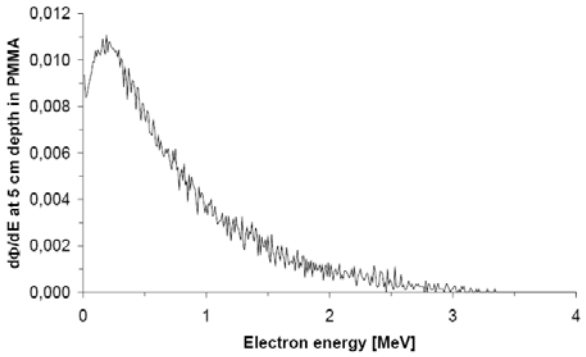

Fig10b Electron fluence at the reference depth in the phantom irradiated with 4MV photons. (After Olsson & Bergstrand 2001).

3.2.6. x-ray irradiation

At the department of Physics and measurement, University of Linköping, an x-ray tube, Philips PW1730 100 kV, was provided in the vicinity of the ESR-spectrometer. A holder for test tubes was contained in a lead shield at the head of the x-ray tube. No calibration had been done using this set up and therefore it was only used for relative dose measurements and qualitative spectrum analysis. The irradiation time varied from half a minute to three minutes, which with the settings 75 kV and 20 mA should correspond to a radiation dose in the order of kGy.

3.3 TISSUE EQUIVALENCE

To calculate the mass energy-absorption coefficients and mass collision stopping power the interactive Internet tables "Tables of X-Ray Mass Attenuation coefficients and Mass Energy-Absorption Coefficients" (Hubbell& Seltzer 1996) and the Internet-executed computer program ESTAR (Berger et al 1998), supplied by National institute of science and technology (NIST), was used. As in-data mass percentage of consistent elements and density of the samples were needed.

The tissue equivalence was evaluated by qualitative analysis of plots of $\left(\mu_{en}(E)/\rho\right)_s / \left(\mu_{en}(E)/\rho\right)_w$ and $\left(S_{coll}(T)/\rho\right)_s / \left(S_{coll}(T)/\rho\right)_w$ and by quantitative comparison of $\overline{\mu}_w^s$ and ${}_m\overline{S}_w^s$ as well as mean weighted coefficients with regard to the different kinds of tissue.

3.4 READOUT

A Bruker ER200D-SRC CW EPR/ENDOR spectrometer was used for collection of all ESR spectra. A Bruker 4102ST/9632 resonance cavity was used for all readouts except for the three months fading experiment with lithium formate where a Bruker ER4116DM/9305 resonance cavity was used. These are TE102 rectangular cavities with a nominal centre frequency of 9.75 GHz and an unloaded Q-factor of 6000.

3.4.1. Spectrometer set-up

The samples were positioned, one at a time, at the bottom of a test tube which was inserted in the resonance cavity from above. The reduction of signal due to vertical displacement has been previously reported to be substantial for an ST-cavity (Anton, 2005). Hence, care was taken to position the sample in the middle of the cavity. A reference marking was put on the test tube so that the positioning could be reproduced. The error of the vertical position was estimated to be ±2 mm. The modulation field is not quite homogenous over the cavity (Nagy 2000a). Thus a change in vertical position of the sample will also have a similar effect to a small change of modulation field.

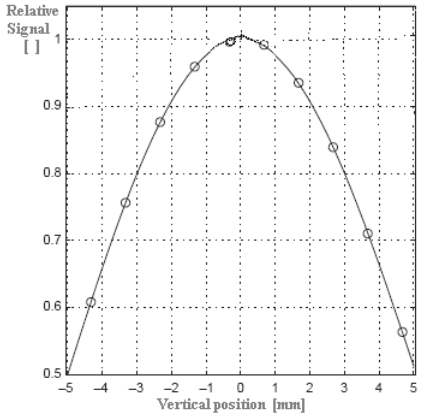

Fig 11a Signal deviation as a function of vertical displacement in the cavity. (after Anton 2005)

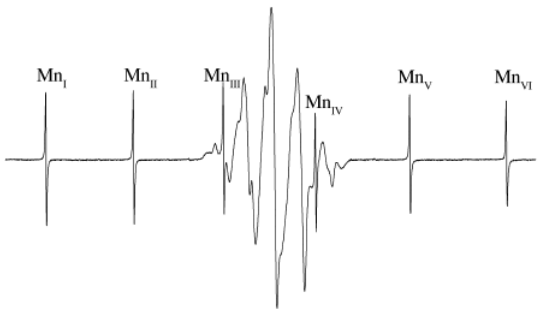

Fig 11b Example spectrum of Ala with MgO(Mn^{2+}) reference. (after Yordanov 2002)

A powder of an Mn^{2+} doped MgO crystal, MgO(Mn^{2+}), was used as a spin concentration reference. The reference was enclosed in a long and thin container which was inserted in the cavity from below. With this arrangement, the bottom of test tube would be in contact with the top of the standard which made positioning of the test tube more accurate.

Spectra from both the sample and reference could be collected simultaneously. This allowed for normalisation of the sample signal and thus the repeatability could be improved (Nagy et al 2000c). The microwave field in the vicinity of the sample has been shown to be disturbed by the reference (Anton 2005). Although the displacement is small the reference will not experience the same field as the sample and thus spin concentration measurements can not be performed with the reference.

The orientation of the pellet can affect the signal due to inhomogeneities in the sample. This effect can be reduced by rotating the sample continuously (Sharpe et al 1996). The present set up did not support this and thus measurements were performed to estimate the orientation effect which was shown to be within two standard deviations of successive measurements of the reference orientation.

3.4.2. Spectrometer tuning

Before readout, the spectrometer was tuned using the following procedure. First, the microwave frequency was scanned to find the frequency of resonance for the cavity, which was identified by an absorption dip on an oscilloscope. The phase of the signal was then adjusted by trying to get a symmetric, non-distorted shape of the absorption dip. At this stage the spectrometer was turned to operate mode and the bias of the detector diode was optimised. Finally, the microwave frequency, signal phase and iris of the cavity were fine-tuned for each setting of microwave power. The described procedure hade to be repeated each time the spectrometer was restarted and every time the sample was changed or repositioned. The manual nature of this procedure contributed to the uncertainty of the reproducibility and although the extent of uncertainty could be reduced by normalisation to the spin concentration reference the impact of this was limited by the reproducibility of the sample positioning relative to the reference and the microwave field.

3.4.3. Spectrometer settings

The spectrometer settings used are presented in table 3. The settings were transferred to the computer in a file and thus the data could be used for automatic processing or analysis described in the following sections.

Table 3 Spectrometer settings

Parameter/quantity	Abbreviation [unit]	Range/typical value
Swept magnetic field	B_0 [mT]	320 - 370
Centre of magnetic field	B_c [mT]	330 - 350
Sweep width	B_w [mT]	30 or 15
Microwave frequency	v [GHz]	9.4 - 9.8
Microwave power	P [mW]	0.5 - 158
Modulation frequency	v_m [kHz]	100
Modulation amplitude	B_m [mT]	0.33 - 2.92
Receiver gain	RG [ ]	5000 -50000
Conversion time	t_c [ms]	81.92
Time constant	[ms]	81.92
Number of channels	n_{ch} [ ]	1024
Number of scans	n_{scan} [ ]	1 - 5

3.5 SPECTRAL PROCESSING

The primary aim of the spectral processing is to cancel the perturbations of the spectrum. As reviewed in the preceding chapter there are both reproducible and a non-reproducible perturbations. The former appear as broad interfering structured deviations of the spectral baseline (Bartolotta et al 1993) whereas the latter appear as non-reproducible baseline drift (Barr et al 1998) or random deviations in each data point. All processing of the spectra were performed on a PC with the program Mathematica®.

3.5.1. Coordinate alignment

Drift of spectrometer settings can cause spectra to be slightly translated along the x-axis. The main cause of translation was found to be instability of microwave frequency. For most purposes the exact location of peaks on the x-axis is of no consequence but for operations like subtraction or fitting of spectra the location is in fact crucial.

The drift was corrected by translating each data point by interpolation of the old channel values. The relative translation could be determined by the location of the peaks of the spin concentration reference in view of the fact that they relate to specific g-values. However, the x-axis resolution of these narrow peaks was low and the deviation of the indicated microwave frequency proved to be a better quantity for correction.

3.5.2. Filtering of the spectrum

Assuming that the pure spectrum from the sample is of intermediate frequency compared to the high frequency noise and the base line drift, the perturbations can be filtered by using a band pass (BP) filter of the fast fourier transform (FFT) of the output spectrum. A BP-filter which cancels the three lowest frequencies as well as all frequencies over the twenty-first has previously been proposed for alanine (Ruckerbauer et al 1996). A more general method, proposed here, is to relate the frequencies that dominate a spectral peak with the peak width, x_{pp}, and n_{ch}. The propositions are based on the fact that the Fourier transform of a Gaussian is also a Gaussian but with the inversed peak width. Thus, the larger the width of a spectral peak is, the lower and more narrow is the frequency band describing it.

The highest low frequency limit (fig12b) which was found not to distort the peak if cancelled is $\Omega_1 \le n_{ch}/5x_{pp}$. The lowest high frequency limit that does not distort the peak if cancelled is $\Omega_2 \le n_{ch}/x_{pp}$. This is also the lowest low frequency limit for complete quenching of a perturbation, $\Omega_1 \ge n_{ch}/x_{pp}^{perturabtion}$. If this is higher than the lower limit for distortion of the sample peak, the signal of the sample and the background overlap in frequency and this method can only be used for filtering random noise with a low-pass filter.

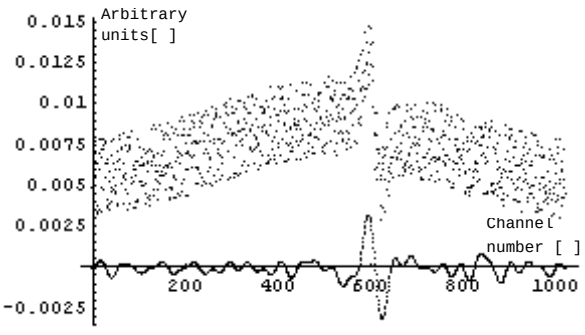

Fig 12a Simulation of a spectral peak, afflicted with heavy perturbation of a broad signal and high frequency noise (points) and the filtrated spectrum (line).

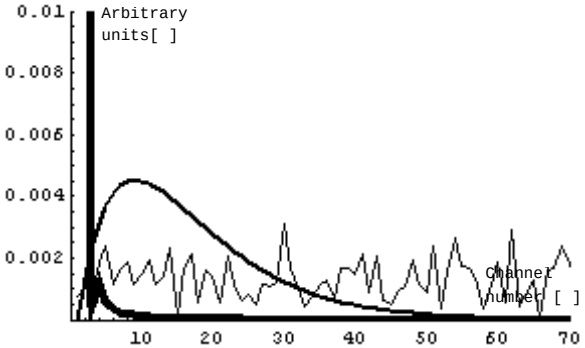

Fig12b Fourier transform of the broad signal (thick line), the spectral peak and the noise (thin line). The frequency limits of the BP-filter, of the proposed method, would be channel 6 & 30.

Blocking frequencies by a step function filter introduces distortions in the spectrum. Thus, for high frequencies a second order Butterworth filter was used. The low frequency region was however too narrow for this approach. The Butterworth filter is

not steep enough to achieve effective blocking of a few samples of low frequencies and thus a step filter had to be used with distortion as an unwanted side effect.

3.5.3. Baseline correction

Another approach to correct baseline drift, more commonly used and commercially adapted, is to fit a polynomial to the distorted baseline and subtract this from the spectrum (Barr et al 1998). However care must be taken not to include the spectral peaks in the fitting. A rule of the thumb used here, is not to use the data points which are closer to the peak centre than 1.5 times x_{pp}. For broad peaks this is a problem since the method gives no information about the baseline drift under the peak. For spectra with several close peaks only the distant parts of the spectrum was used for the fitting.

3.6 ANALYSIS OF THE SPECTRUM

The qualitative analysis of the spectrum involves identification of number, shape and positions of spectral peaks. This procedure could be part of an automatic computer algorithm but in practise implementation of such an algorithm is hard when the details of the spectrum are unknown. Thus a subjective classification of spectral details such as multiple overlapping peaks, interfering peaks or baseline distortion had to be carried out before automatic quantification could be performed.

3.6.1. Quantification of the spectral peak

A simplified peak quantification algorithm was implemented in Mathematica®. The region where a peak or a number of peaks was expected and the indicated spectrometer parameters were used as input. In that region the algorithm used non-linear fitting of a gaussian derivative shape function to the data y^x. A local baseline correction was included by adding a linear component to the shape function before the fitting. The values of the fitted shape function, v^x, were assumed to resemble the ESR-spectrum. The fitting yielded estimates of signal v_{pp}, the peak width B_{pp} and location B_r from which the g-value could be calculated. The algorithm could handle simple deconvolution but was unable to account for non-symmetric or non-gaussian peaks.

3.6.2. Uncertainty of the ESR-signal

Although the readout and influence parameters are known not to be independent variables of the readout signal v_{pp}, they were assumed to be so for the calculations of uncertainty. This was because of the insufficient knowledge of their co-variation. The uncertainties due to readout or influence parameters were estimated by type B evaluation while the uncertainties due to non controllable variations in readout and spectral processing as well as variations between dosimeter samples were estimated by type A evaluation. The uncertainties were estimated both for repeated and reproduced measurements, were the former refers to unchanged sample position and spectrometer tuning as well as no expected change in environmental conditions.

The uncertainty in sample position results in deviations for both effective P and B_m over the sample. The effect of this to v_{pp} was estimated from fig11a (Anton 2005) for P and from measured deviation of B_{pp} of the reference for B_m. The latter estimation was performed at high B_m, using the fact that B_{pp} is a linear function of B_m for B_m much higher than λ_{pp} (fig6b). Assuming rectangular distribution of the positioning, the uncertainty was estimated to be 2.2% for P and 4.5% for B_m, resulting in a combined uncertainty of 5.0%.

The uncertainty due to variation in Microwave frequency v was estimated from the standard deviation of indicated v, assuming normal distribution. For the quality factor of the resonance cavity Q, the uncertainty was estimated from the data of Nagy (2000c) including realistic variations in humidity for reproducibility and excluding it for repeatability. The data from the same publication was used for uncertainty of Receiver gain (*RG)*.

For variations due to temperature of the sample T, the measured standard deviation of T in the cavity was used for calculation of uncertainty using Eq17. No attempt was made to include temperature variation of relaxation times or co-variation with humidity affecting the uncertainty due to variation in Q.

The uncertainty due to variation of P was estimated through the standard deviation of the signal below saturation minus the standard deviation at P_{max} (where no variation due to P is expected). The estimate is of the same order as previously has been reported for other equipment (Maier & Schmalbein 1993). For B_m the uncertainty was estimated from standard deviation of B_{pp} (for high B_m) of the reference for B_m. In both cases normal distributions were assumed. For signals normalised by the reference the uncertainty is not zero for saturated and over modulated samples but rather a function of the saturation and modulation behaviour of sample compared to the reference (Nagy et al 2000c). This was estimated from Eq23) and 24b fitted to the optimisation data (see sub section 3.7.5).

The data obtained from the spectral dose response model (See sub section 3.8.3) were used to estimate the uncertainty due to non-controllable variations in readout and spectral processing. This was performed by subtracting the reproducible BGS and SBG signals from a series of spectra and calculating the standard deviation of v_{pp} which was established to be 3.1%. After corrections for the contributions due to the readout and the influence parameters stated above, the uncertainty was reduced to 2.5%. From the same body of data the variation of v_{pp} for different dosimeters was calculated to be 6.4% but was reduced to 3.1% after correction for uncertainty of influence parameters of reproduced measurements and uncertainty of dosimeter mass.

Table 4 Sources of uncertainty of v_{pp}

Uncertainty of v_{pp} due to deviation of:		Reproduced measurement [%]	Normalised to reference [%]	Repeated measurement [%]	Normalised to reference [%]
δv_h	Vertical position, h	5.0	5.0	-	-
δv_v	Microwave frequency, v	0.5	-	0.1	-
δv_P	Microwave power, P	2	0.2	2	0.2
δv_{Bm}	Modulation amplitude, B_m	2	0.7	2	0.7
δv_Q	Quality factor, Q	7	1	1	-
δv_T	Temperature of the sample, T	2	-	1	-
δv_{RG}	Receiver gain, RG	2	-	2	-
δv_{ro}	Readout and processing	2.5	2.5	2.5	2.5
δv_s	Dosimeter sample	3.1	3.1	3.1	3.1
δv_{pp}	**Total uncertainty**	**10**	**6.5**	**5.5**	**4.0**

The contributions to uncertainty of the ESR-signal v_{pp} are presented in table 4. The total uncertainty was estimated to be 10% for reproduced and 5.5% for repeated measurements. By normalisation to reference the uncertainties were 6.5% and 4.0% respectively. Summation of spectra from repeated measurements (see sub-section 2.2.3) would reduce the uncertainties by the square root of the number of scans n_{scan}, although the practical limit of this reduction due to non random errors was not established.

3.6.3. Integration of the spectrum

If the modulation amplitude is low enough to avoid distortion the output spectrum is the derivative of the absorption spectrum. Thus the double integral (Barr et al 1998) of the output spectrum can be used for calculation of the radical yield independent of the spectral shape. The double integral was calculated according to $I = B_w / n_{ch} \sum_{i=1}^{k_{ch}} \sum_{x=1}^{i} y^x$.

3.7 OPTIMIZATION OF READOUT PARAMETERS

Spectra were collected for P=0.5, 1, 4, 10, 20, 40, 80 and 158 mW and at each of these settings for B_m=0.33, 0.73, 1.04, 1.64, 2.07, 2.61 and 2.9 mT. These data were used to compare three different methods of optimization.

3.7.1. The careful method

The aim of the careful method is to optimize the readout parameters while avoiding power saturation and over modulation. Thus, v_{pp} should increase linearly with B_m and linearly to the square root of P. The careful method need to be used if the spectra should be used for spin concentration measurements (Jiang, 1998). The constraints used in the present study are that the deviation from linearity should be less than 10%. This would result in at most 10% less accuracy of normalisation to a spin concentration reference in the linear region (Nagy et al 2000c).

3.7.2. The standard method

Optimization of v_{pp} without concern of saturation or over modulation is usually performed by first keeping B_m fixed at a low level while the P is gradually increased until the v_{pp} cease to increase. Then B_m can be increased in the same manner (Jiang,

1998). With this method, henceforth called standard method, it is often possible to find optimal parameters in just a few measurements.

3.7.3. The matrix method

The standard method does not account for the fact that P and B_m are not independent variables of the signal response. An alternative method is to vary the modulation amplitude for each value of microwave power, thus obtaining a matrix of ESR-signals (Olsson et al 2002a). The maximum signal obtained by this method is then chosen to be the optimum. This method requires much more measurements but has been shown to reach optima of higher sensitivity (Vestad et al 2003).

3.7.4. Relative nature of parameter optima

According to the reviewed theory the optimal readout parameters are relative to the spectrometer characteristics, influence quantities and the irradiation situation. The saturation behaviour is characterised by P_0 which is a function of spectrometer characteristics, such as Q (Gallay & Van Der Klink 1986). Thus, the value of P_0 is relative to the type of cavity and is error prone to the tuning and the influence of humidity (Nagy et al 2000c). Furthermore, high LET radiation has been shown to result in slightly shorter T_2 (Lund et al 2004, Malinen et al 2006) and thus higher P_0 and larger λ_{pp}. The increase of the latter quantity will result higher optimal values of B_m.

3.7.5. Model of data fitting

For graphic presentation of the data for optimisation as well as some of the estimations of uncertainty it was useful to fit the data to Eq23, 24a and 24b. This was performed by the non linear fitting algorithm of Mathematica™.

3.8 SENSITIVITY OF THE DOSIMETRIC SYSTEM

The sensitivity of an ESR dosimeter is the product of the radiation sensitivity and the spectroscopic sensitivity. If it is the dose in the surrounding material that is of interest the cavity theory relation also need to be included.

3.8.1. Dose response

Conventionally dose response measurements in ESR-dosimetry are made using linear regression of v_{pp} normalized by the dosimeter mass $l_i = \left(v_{pp}\right)_i / m_i$. The regression was performed according to (12).

The uncertainty of each normalized signal is $\delta l_i = l_i \sqrt{\delta m_i^2 / m_i^2 + \delta\left(v_{pp}\right)_i^2 / \left(v_{pp}\right)_i^2}$. If the uncertainties of D are not negligible compared to l, the linear regression should be performed according to the effective variance method (Orear 1982) previously proposed for calibration of ESR dosimeters (Bergstrand et al 1998). In the present study, however, the uncertainties of l was much larger than those of D.

3.8.2. Linearity of dose response

The standard test of linear regression is the coefficient of determination R^2 which should be close to unity for a good fit. It must be noted that R^2 is not just a measure of the goodness of the linear model but also a measure of the variance of the data. Thus it must be complemented with specific analysis of the variance. For the linear regression the variance, which is square of the standard uncertainty u, is given (Bergstrand et al 1998) by

$$u^2(l) = (n-2)^{-1} \sum \left(l_i - l_0 - aD_i\right)^2 \tag{29a}$$

$$u^2(l_0) = u^2(l) n^{-1} s_D^{-2} \sum D_i^2 \tag{29b}$$

$$u^2(a) = u^2(l) s_D^{-2} \tag{29c}$$

with the mean value of all dosimeter doses $\overline{D} = n^{-1} \sum D_i$ and the squared deviation from the mean of all dosimeter doses $s_D^2 = \sum \left(D_i - \overline{D}\right)^2$.

3.8.3. Spectral dose response model

A more general method for dose response which evaluates the dose correlation of the entire spectrum is proposed here. A similar approach has been previously used for archaeological dating (Grün 1998). For the moment the uncertainty of the dosimeter doses and masses are neglected. Furthermore the dose response is assumed to be linear. Later the uncertainties will be taken into account and the validity of the assumption will be tested by independent methods.

A series of spectra from dosimeters of varied dosimeter mass and absorbed dose was used as input. The dose response for each spectral point *x* was be calculated by linear regression of Eq26. Hence, first the spectrometer signals of the first channel in all spectra were fitted to a linear function of dose, dosimeter mass and background and then the procedure was repeated for each channel until the entire spectrum was covered.

The regression was executed with a self developed Mathematica® program and resulted, for each data point *x,* in a dosimeter independent value (*x,* a^x_{SBG}), a zero dose value (*x,* a^x_{BGS}), the slope of the dose response curve (*x,* a^x_{RIS}) and the coefficient of determination of the linear regression (*x,* $(R^2)^x$).

3.8.4. Sensitivity

Using either dosimeter dose or dose to the surrounding material, the total sensitivity can be evaluated by using the result of the linear regression (Eq12) and defining sensitivity as $S = a$ (Bartolotta et al 1993). The expanded uncertainty for sensitivity is $U(S) = k \cdot u(a)$, using the coverage factor *k*=2 for 95% confidence interval. The zero dose (Bartolotta et al 1993) is the dose that the signal of an unirradiated dosimeter would correspond to, $D_0 = l_0 / a$, if not corrected with the constant factor of the linear regression. The expanded uncertainty of zero dose is, as for sensitivity, $U(D_0) = k \cdot D_0 \sqrt{u^2(l_0)/l_0^2 + u^2(a)/a^2}$. A final quantity, related to the sensitivity is the lower limit of distinguishable dose difference which is called dose resolution and defined as three standard uncertainties of *l* divided by the sensitivity, $R = 3u(l)/S$ (Bartolotta et al 1993). Because of the limited and unequal number of data points for each material, *R* should not be viewed as characteristics of the dosimeter materials but as a measure of deviation of single readouts of individual dosimeters compared to the linear regression.

The lower limit of detection (LLD) has previously been defined as the lowest dose which is significantly different from the background noise (Bartolotta et al 1993). This was evaluated as the dose which the signal of three standard deviations of the

background noise would correspond to, according to the sensitivity, for a *0.05 g* dosimeter.

3.8.5. Radiation chemical yield

The radiation yield can be calculated if N_v and dosimeter dose is known. Consequently a common practice is to normalize the double integral of the sample output signal to that of a spin concentration standard measured simultaneously in the spectrometer cavity. In the present study, as mentioned above, equal positioning and geometric shape to the spin concentration reference could not be obtained with the available cavity setup. An alternative method, used in the present study, is to use another irradiated material with known radical yield as reference dose standard. The radiation chemical yield can then be calculated from the fraction of the double integrals for the investigated sample, I_X, and Ala as a reference. Both samples were normalised to the spin concentration reference.

$$G(X) = \frac{(I/I_{Std})_X}{(I/I_{Std})_{Ala}} \frac{(mD_s)_{Ala}}{(mD_s)_X} \cdot G(Ala) \qquad (30)$$

The spectrometer settings need to be well below those for saturation and over modulation.

3.8.6. Radical stability of the dosimeter material

Fading is studied by, immediately following x-ray irradiation, placing the sample in the cavity, where it is fixed until all series of measurements for that sample are completed, and begin the readout as soon as the tuning of the cavity is completed. During the first 15 minutes, a new spectrum was collected every two minutes, which is close to the practical limit of the scan time. After this, a spectrum was collected every 15 minutes for several hours. The aim of this procedure was to detect rapid radical dynamics. For long term fading analysis, one series of measurement was preformed ones a weak after the first hours of measurement described above. To cancel variations in spectrometer settings the signal was normalised (see sub-section 2.3.4 & 3.4.1), yielding the quantity v_{Mn}^X. Every readout was also normalized to the first recorded value at time t_0 after irradiation, $v_{t_0}^t = \left(v_{Mn}^X\right)_t / \left(v_{Mn}^X\right)_{t_0}$.

Guided by the review in sub-section 2.4.4 the fading is assumed to be exponential and hence exponential regression was used to fit the $v_{t_0}^t$ data. A logarithmic plot of $v_{t_0}^t$ should be linear for a good fit. Presence of knees in the logarithmic plot is an indication that there are several radicals with different fading time that contribute to the spectrum. If this would be the case, non-linear fitting with a sum of exponential functions should be used.

4. RESULTS AND DISCUSSION

4.1 DOSIMETER MATERIALS

The pellets of LiFo and NaFo were strong whereas the salts of lactic acid were fragile in pure powder form. The powder of the lactates was mixed with paraffin (5% of the weight of the pellet) before pressing the pellets. By omitting the binding material for the formates the sensitivity of the dosimeters could be increased (Vestad et al 2003). The pellets of KFo became partly dissolved in air a few hours after fabrication and were thus excluded from the study.

4.1.1. Tissue equivalence of dosimeter materials

The mass energy-absorption coefficients (fig13a) of LiFo are lower than that of Ala in the radiotherapy energy region but the general energy dependence of LiFo is more linear with tissue. For NaFo the coefficients are only close and linear in a region around 1 MeV. The abrupt energy dependent behaviour outside this region is due to the higher atomic number of the cations. The situation for mass collision stopping power coefficients (fig13b) is similar. Ala is closest to tissue but LiFo is more linear. The coefficients of NaFo are lower than LiFo for all energies studied but increase with energy.

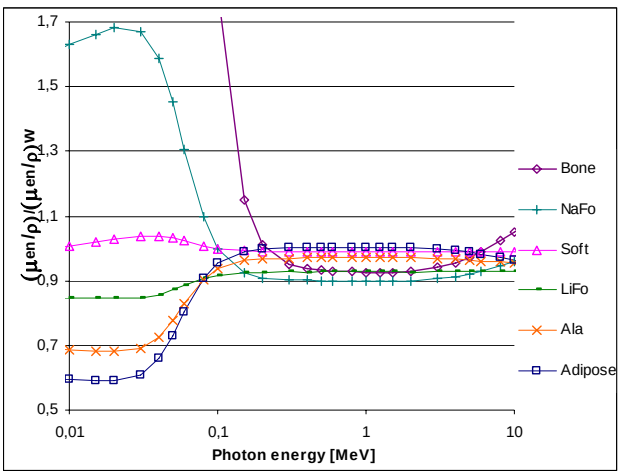

Fig13a Log-Lin plot of mass energy-absorption coefficients as a function of photon energy

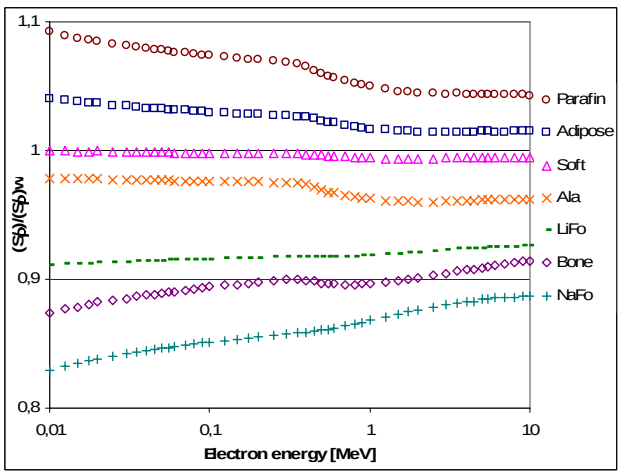

Fig13b Log-Lin plot of mass collision stopping power coefficients as a function of electron energy.

The mean weighted coefficients for a 4 MV photon (table 5) field indicates that LiFo is close to water but not as close as Ala. These calculations assume that Ala is mixed with

5% paraffin. Mixing LiFo and NaFo with paraffin would of course improve the tissue equivalence although it would reduce the sensitivity.

Table 5 Mean weighted coefficients of mass energy-absorption coefficient and stopping power, for a 4 MV photon beam.

Material	$(\bar{\mu}_{en}/\rho)_w^s$	${}_m\bar{s}_w^s$
LiFo	0,927	0,915
NaFo	0,902	0,863
Ala	0,970	0,969

Assuming that the same photon energy fluence and electron particle fluence as in water the modifying factor for the dosimeters as cavities in different kinds of tissues was calculated (table 6). For soft- and adipose tissue the trend is the same as for the mean weighted coefficients. For bone LiFo is very close to unity. Although the validity of the previous assumption for the fluence could be put in question in this case, this indicates LiFo dosimeters are good candidates for *in vivo* dosimetry.

Table 6 Modifying factors according to the cavity theory of Burlin (1966) for different kinds of surrounding tissue in a 4 MV photon field and a dosimeter of size and shape described in sub-section 3.1.1

	f_H2O	f_Soft	f_Adipose	f_Bone
Ala	0,97	0,98	0,96	1,07
NaFo	0,88	0,88	0,87	0,96
LiFo	0,92	0,93	0,91	1,01

4.2 ESR SPECTRA

For LiFo and NaFo intense spectral peaks were found (fig14a and b). No detectable signal was obtained for LiLa or CaLa. Consequently these substances were rejected in the further studies. The absence of signal of LiLa is however in contrast to previous studies (Hassan et al 1997, Hassan & Ikeya 2000 and Hassan & Ikeya 2002). No part of the reviewed methods has been found to be the source of the contradicting results and the results for lithium formate compared to previous studies speak in favour for the reviewed methods. Thus the contradiction remains dubious and further investigation is needed. ZiLa had a complicated spectrum (fig14c) and weak signal intensity in the peaks. Change of readout parameters did not improve the signal much. Therefore ZiLa was also rejected in the further studies.

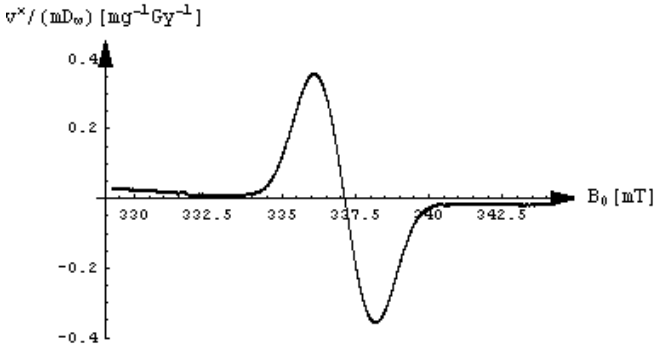

Fig14a Spectrum of LiFo at P=80 mW, B_m=2.92 mT

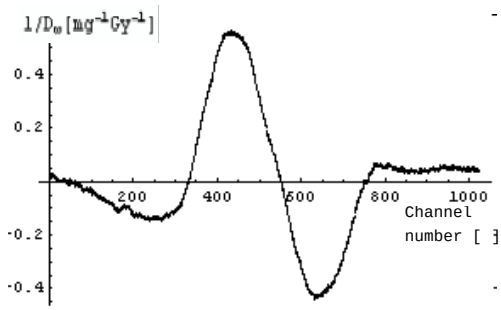

Fig14b Spectrum of NaFo at P=158 mW, B_m=2.92 mT

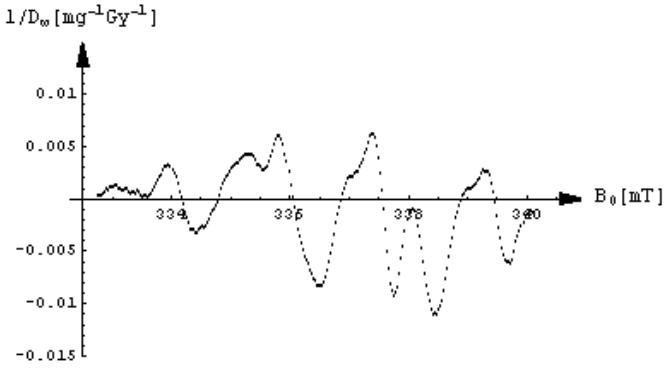

Fig14c Spectrum of ZnLa at P=2 mW, -B_m=0.37 mT

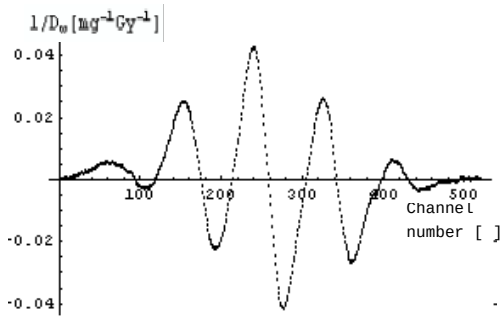

Fig14d Spectrum of Ala at P=8 mW, B_m=1.47 mT

4.2.1. Spectral processing

The proposed filter method showed to be very efficient. Processing of 56 spectra for each of Lifo, NaFo and Ala only required 20 lines of Mathematica® code and no user input was needed during some 30 s of processing on a common PC. Furthermore the method is objective. However for spectral peaks that are broader than one tenth of the scanned spectrum, the filtering distorts the spectrum (fig15d). This is probably due to insufficient number of channels of the FFT for a broad peak. Furthermore, the method is useless if the perturbation interferes with the spectral peak in the frequency domain.

Although more complicated, much slower and subjective, the baseline correction method works well as long as there is enough baseline sufficiently far from spectral peaks in the spectrum.

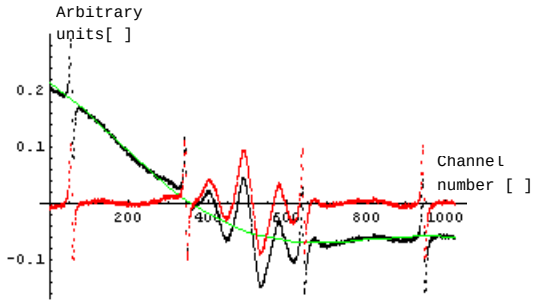

Fig15a Conventional baseline correction, of the perturbated spectrum of Ala, by subtracting a baseline fitted 6th order polynomial.

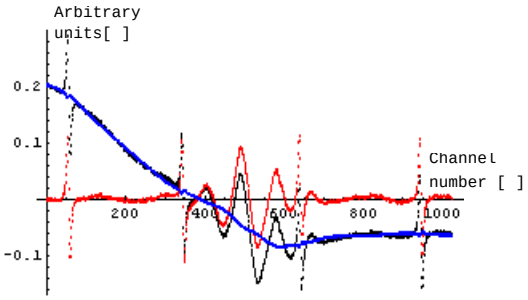

Fig15b BP-filtering of the perturbated spectrum of Ala

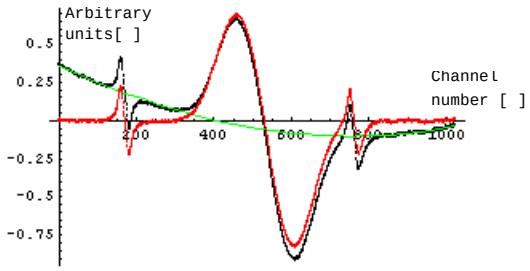

Fig15c Same as 15a but with LiFo and half the scan width. The fitting is more difficult because only limited parts of the spectrum can be used for the polynomial fit.

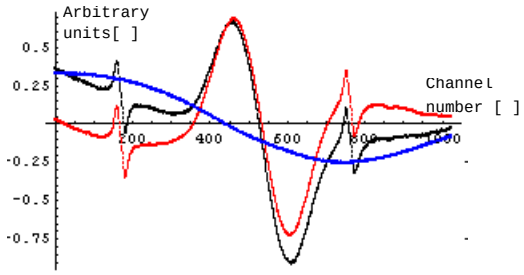

Fig15d BP-filtering of the perturbated spectrum of LiFo resulting in heavy distortion due to insufficient spectral width compared to peak width of LiFo.

For dose assessment of samples with well known spectral characteristics an indirect approach could improve the results by subtracting the estimated dose spectrum, fitting a polynomial function to the baseline, subtracting this from the original spectrum and then make a new estimate of the dose spectrum. By iterating this procedure the baseline influence on the dose estimate can be reduced (Sharpe et al 1996).

4.2.2. Spectral analysis

The single broad spectral peak of LiFo (fig 14a) has in former studies been shown to be the result of inhomogeneous broadening due to hfs of the Lithium nucleus (Vestad et al 2004a) which has two common isotopes (table 7). The unpaired electron will be situated at the carbon atom. However the only carbon isotope resulting in hfs is ^{13}C, which has a small natural abundance, and therefore the spectrum of this atom, is rarely detectable. The absence of such satellite peaks in the present study is hence not contradicting. The orbitals of oxygen are supposed to be spin polarized by the unpaired electron at the carbon atom (Vestad et al 2004a) but same reasoning applies to the isotope ^{17}O.

Table 7 Isotopes of the analysed substances that have net nuclear spin, presented with natural abundance

Nuclear spin	Isotope
½	^{1}H (99,9%), ^{13}C (1,1%)
1	^{6}Li (7,5%)
3/2	^{7}Li (92,5%), ^{23}Na (99,9%)
5/2	^{67}Zn (4,1%), ^{17}O (0,04%)

For NaFo hfs-structure is found at low modulation amplitude but at higher amplitude the peaks are super positioned as a result of modulation broadening (16a). The result is similar to that obtained for the modulation amplitude dependence of L-alanine-d_4 (Gancheva et al 2006). This interpretation of the result was supported by a simulation of modulation broadening of four ^{23}Na peaks (fig 16b).

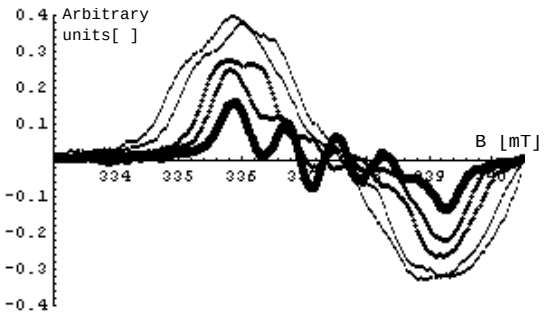

Fig16a Modulation broadening effect to hfs-structure of NaFo. Thinner graphs represent higher modulation amplitude.

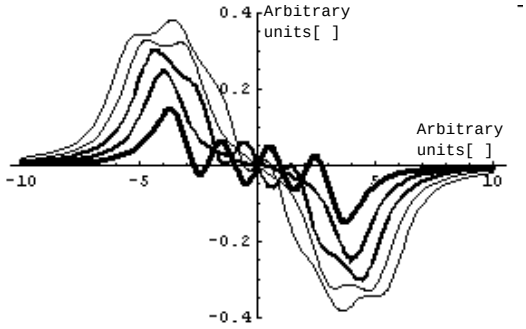

Fig16b Simulation of modulation broadening for hfs of ^{23}Na.

4.3 OPTIMAL READOUT PARAMETERS

Three strategies for optimization were compared. The careful method could not be employed for NaFo with the available spectrometer settings because distortion due to modulation was present even at the lowest value of B_m. Because of the overmodulation behaviour of NaFo, described in the previous section, it was most practical to use the difference between the outermost peak lobes for the optimization, since these were the only peaks that were preserved at high modulation (fig 16a).

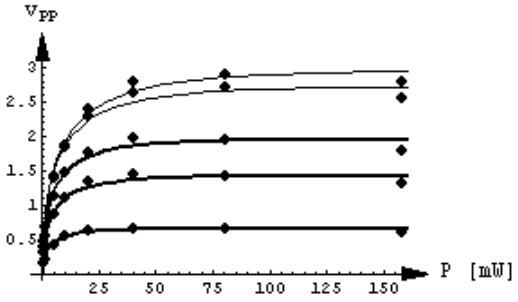

Fig17a. Fitting of the optimization data for LiFo. Thinner graphs indicate higher B_m ranging form 0.33 to 2.07 mT

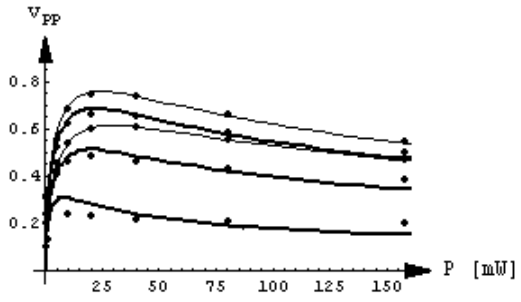

Fig17b. Fitting of the optimization data for Ala. Thinner graphs indicate higher B_m ranging form 0.33 to 2.07 mT

For LiFo and Ala both the standard- and matrix method yielded considerably higher signal amplitudes than the careful method and thus for dosimetric purposes it is sensible to operate the spectrometer at saturation and overmodulation. The Matrix method allowes much higher spectrometer settings but because of intense saturation and overmodulation the signal does not increase as much. For LiFo the increase is within the uncertainty of the measurement.

Table 8 Optimal spectrometer settings and signal for different optimization methods,

	Method	P [mW]	B_m [mT]	I/D [g^{-1} Gy^{-1}]	$I_{opt}/I_{P=0.5,Bm=0.33}$
LiFo	Careful	5	0.73	0.14±0.02	5.4
LiFo	Standard	40	2.07	0.74±0.08	17.5
LiFo	Matrix	80	2.61	0.78±0.08	18.5
NaFo	Standard	20	2.92	0.60±0.06	13.3
NaFo	Matrix	80	2.92	0.79±0.08	17.3
Ala	Careful	1	0.33	0.022±0.003	1.5
Ala	Standard	5	1.64	0.088±0.009	5.5
Ala	Matrix	20	1.64	0.12±0.02	8.2

The results of all substances confirm that the P and B_m are not independent variables, as predicted by Brotikovskii et al (1973). As the co variation is also dependent on

modulation frequency (Bloembergen et al 1948, Portis 1953) the validity of the result is limited to the current settings of 100 kHz. Furthermore, the value of the spin relaxation parameter P_0 depends on the conversion factor c of the cavity (Sagstuen et al 2000) which is a function of the Q-factor and filling factor η (Gallay & Van Der Klink 1986). Hence, in absolute values the validity is limited to the present cavity and dosimeter shape. These facts probably explain the discrepancy between the parameter optimization for LiFo of Vestad et al (2003), Malinen et al (2004) and the present study.

All methods presented here aimed at optimising the signal intensity, which is in fact arbitrary. If the saturation and over modulation behaviour of the reference is different, the uncertainties of normalisation to spin concentration reference increases (Nagy et al 2000c). Furthermore, the increase of interfering background signals might be larger than the increase of the signal of dosimetric interest. Thus, the accuracy of absorbed dose need not be optimal at optimal signal intensity. Less relative measures for optimisation would be to minimise the relative contribution of background signals (BGS or SBG) compared to the signal with dose information (RIS). Minimisation of the statistical deviation of RIS could also be an adequate measure. A preliminary test with just four different parameter settings (Table 9) indicates that operating at saturation and over modulation is justified, even though the parameter should be more moderately set than indicated by the maximum intensity approach.

Table 9 Different measures of optimal sensitivity at different spectrometer settings of LiFo dosimeters with the mass of 0.05 g

P [mW]	B_m [mT]	$l_{BGS}/(l_{RIS}/D)$ [Gy]	$v_{SBG}/(v_{RIS}/D)$ [Gy]	$\delta(l_{RIS}/D)$ [%]
1	0.73	5,2	7,9	3,2
8	1.47	2,7	4,6	3,1
10	2.07	2	3,9	1,5
80	2.92	1,7	4,3	5

Alternative approaches such as to optimise dose equivalent of the noise (NsD) (Ivannikov et al 2002) has been proposed. Of even more importance would be to optimise a quantity which minimizes the uncertainties of calibration or dose assessment. Statistical measures such as the standard deviation of the determined doses (SDD) (Ivannikov et al 2002) could suffice.

4.4 DOSE RESPONSE AND SENSITIVITY

4.4.1. Dose response

The method of dose response measurement by linear regression of each data point of the entire spectrum (as proposed in sub-section 3.8.3) produced spectra of dose dependence for unit dosimeter dose and mass (fig18a). From peak fitting of the obtained spectra spectral characteristics could be calculated (table 10).

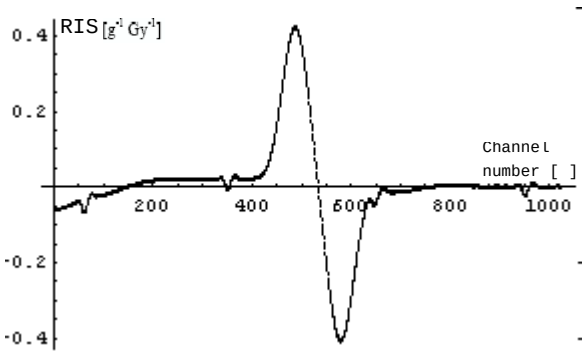

Fig18a Dose dependence of LiFo spectrum at P=80 mW, B_m=2.92 mT

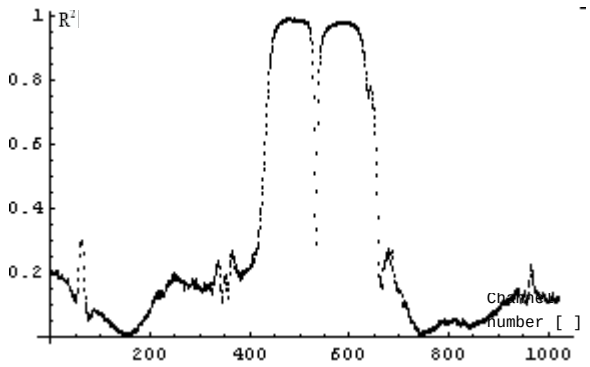

Fig18b Coefficient of determination of the linear regression for LiFo

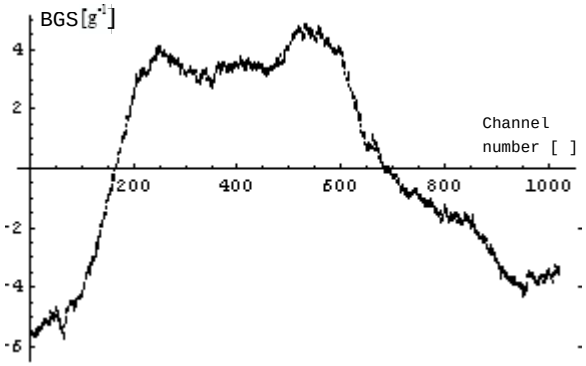

Fig18c Mass dependent background signal of LiFo spectrum

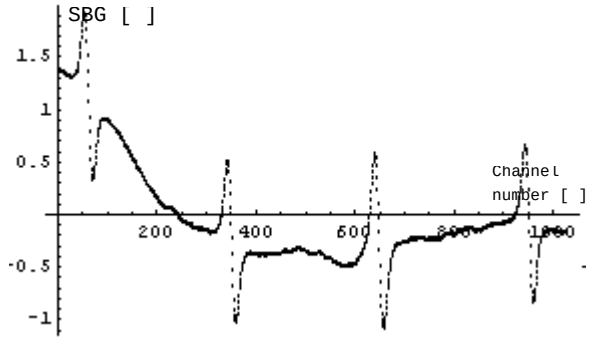

Fig18d Dosimeter independent background signal

The coefficients of determination (R^2) were also plotted (fig18b) as an indication of the accuracy of the dose response measurement. They show good accuracy of dose dependence plots but poor accuracy of the background signals (fig18c & d). The method allowed separation of the background signal in the part stemming from background signal from the sample itself (fig18c) and from the spin concentration reference, test tube and spectrometer (fig18d). A wider range of dosimeter mass and more data is however needed to achieve accuracy of this practise.

Table 10 Dose response and spectral data for LiFo, NaFo and Ala

	P [mW]	B_m [mT]	l/D [g^{-1} Gy^{-1}]	B_{pp} [mT]	B_r [mT]	g [ ]
LiFo	80	2.92	0.71	2.11	337	2.00
NaFo	158	2.92	0.23	3.02	337	2.01
Ala	8	1.47	0.084	1.08	337	2.01

4.4.2. Linearity of dose response

The linear regression was well within the uncertainties of *l*. The uncertainty of *D* was, as noted in sub-section 3.8.1, far less and was therefore neglected.

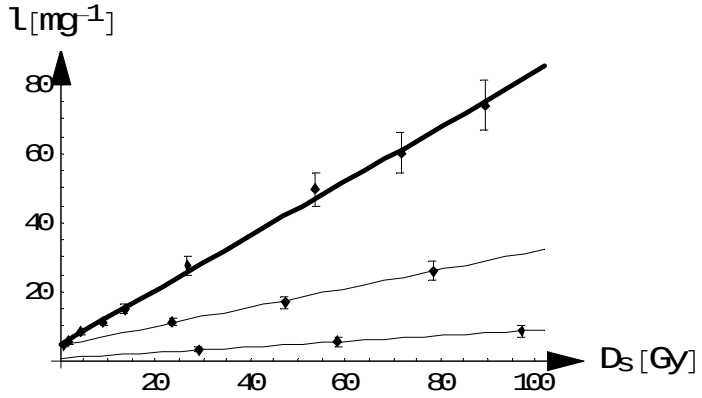

Fig19a. Dose response in water equivalent phantom for LiFo (thick graph), NaFo and Ala (thin graph).

The coefficients of determination (table 11) of the linear regression (Fig19a and b) and the uncertainty of the sensitivity (table 12 and 14) indicate that the dose response is linear for all three materials within the therapeutic dose range.

Table 11 Coefficient of determination of linear regression

Material	LiFo	NaFo	Ala
R^2	0.992	0.972	0.991

4.4.3. Sensitivity

The sensitivity *S* for measurement of absorbed dose to water (table 12) for LiFo is 9 times higher than that of Ala. The sensitivity of the dosimeter material itself is 9.5 times higher. This is higher than previously reported (Lund et al 2002 and Vestad et al 2003) but higher values of *P* and B_m has been used in this study. For NaFo the same quantities are 2.5 and 3 times higher than for Ala. This seems to be in contrast with the intensities for NaFo during optimization of readout parameters but is in fact a result of the rapid

fading of NaFo (see section 4.6). Actually, the difference corresponds very well to the obtained half life of the NaFo radical (fig21b).

Table 12 Sensitivity of the readout compared to dose to water using conventional baseline correction method and the filter method

			Conventional method			Filter method		
	P [mW]	B_m [mT]	S [g^{-1} Gy^{-1}]	D_0 [Gy]	LLD [Gy]	S [g^{-1} Gy^{-1}]	D_0 [Gy]	LLD [Gy]
LiFo	80	2.92	0.71±0.02	6.7±1.4	0.10	0.67±0.02	6.1±1.3	0.07
NaFo	158	2.92	0.21±0.04	22±12	0.19	0.20±0.04	16±13	0.14
Ala	8	1.47	0.078±0.007	12.8±6.6	0.25	0.078±0.008	11.0±7.0	0.24

The difference of sensitivity when using the filter method (table 12) is only a few percent for LiFo and NaFo. For Ala the two methods resulted in the same sensitivity. Both zero dose D_0 and S are lower for the filter method although it is not clear whether this is an indication of exaggerated or more accurate baseline correction. The lower limit of detection (LLD) improves significantly with the filter method.

The quantity D_0 is obviously not a dose quantity but is given the unit gray because of the division of the zero dose signal by the sensitivity. It should be interpreted as the measured dose it would correspond to if no correction of the zero dose signal was performed. Even if such a correction is performed the accuracy of low doses is prone to errors due to the uncertainty of D_0. The obtained values of zero dose uncertainty are not comparable measures for the different substances because of the different number and distributions of measurements. For NaFo and Ala only six dosimeters were measured and no dosimeters were irradiated at doses lower than 30 Gy. Thus, the uncertainties of D_0 should rather be viewed as measures of the accuracy of the dose response curve. The dose resolution R (table 13, 14 & 15) refers to the resolution of two dosimeters from a single readout of each. Although both R and the uncertainty of D_0 are very high their values are significantly reduced by repeated readouts in practical measurements. In the present study the effect of repeated readouts is only exemplified (table 13, 14 & 15) whereas the minimal obtainable values should be the subject of future studies.

The higher values of sensitivity for dose of the dosimeter material as compared to dose to water (table 12 & 13) are due to the fact that the modifying factors used for dose calculations are less then unity. This is more pronounced for the formates.

Table 13 Sensitivity of the readout compared to dosimeter dose. The lower values of D_0 and R obtained due to two successive readouts are included in parentheses as an example how non-destructive readout of ESR can be used to improve the accuracy.

	P [mW]	B_m [mT]	S [g^{-1} Gy^{-1}]	D_0 [Gy]	LLD [Gy]	R [Gy]
LiFo	80	2.92	0.79±0.02	6.0±1.2 (0.8)	0.07	8.7 (5.4)
NaFo	158	2.92	0.27±0.05	17.2±9.7 (4.3)	0.10	14 (6.2)
Ala	8	1.47	0.080±0.008	12.3±6.5 (4.2)	0.20	9.6 (6.3)

The sensitivity for LiFo at varied readout parameters (table 14) is in agreement with the results from the readout parameter optimization. The data in table 14 are not from the same dosimeters or session of measurement which explains difference of D_0 compared to table 13. Although S and LLD are improved with higher readout parameters this is not the case for D_0 or R. This is a further indication of the need for alternative optimisation criteria as mentioned in section 4.3.

Table 14 Sensitivity at different spectrometer settings of LiFo.
The lower values of D_0 and R obtained due to two successive readouts are included in parentheses.

P [mW]	B_m [mT]	S [g^{-1} Gy^{-1}]	D_0 [Gy]	LLD [Gy]	R [Gy]
1	0.73	0.11±0.01	1.8±2.7 (1.3)	0.45	9.9 (4.8)
8	1.47	0.45±0.03	1.8±3.1 (1.5)	0.12	11 (5.3)
10	2.07	0.53±0.03	1.6±3.1 (1.7)	0.11	12 (6.2)
80	2.92	0.80±0.04	1.8±3.0 (1.4)	0.08	11 (5.3)

The background signal of the dosimeter material (BGS) and the spectrometer (SBG), obtained from the dose response measurement by linear regression of the entire spectrum (se sub-section 4.4.1), were used as an alternative to baseline correction. The result (table 15) was almost the same as the previous with regard to sensitivity but the uncertainties were reduced. The result would probably been even better if more dosimeters irradiated at lower doses and with a larger variety of dosimeter mass had been used for the dose response regression analysis.

Table 15 Sensitivity at different spectrometer settings of LiFo when the spectra are corrected by the BGS and SBG spectra.
The lower values of D_0 and R obtained due to two successive readouts are included in parenthese.

P [mW]	B_m [mT]	S [g^{-1} Gy^{-1}]	D_0 [Gy]	R [Gy]
1	0.73	0.11±0.003	0.8±1.7 (0.7)	6.1 (2.5)
8	1.47	0.43±0.01	0.2±1.8 (1.0)	6.7 (3.6)
10	2.07	0.51±0.02	0.9±1.9 (1.0)	7.0 (3.6)
80	2.92	0.80±0.03	0.1±1.7 (0.9)	6.3 (3.3)

4.5 RADIATION CHEMICAL YIELD

Because of the relative nature of the present radical yield measurement the accuracy could not be established. Furthermore, too few measurements were performed for meaningful determination of the precision. The type B uncertainty due to positioning as well as to baseline correction and integration processes (fig 20 a & b) was estimated as to be as high as 20%.

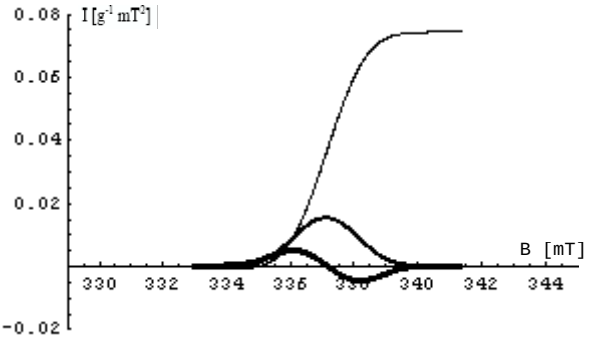

Fig20a Output spectrum (thick graph), integral resembling the absorption spectrum and double integral (thin graph) for LiFo

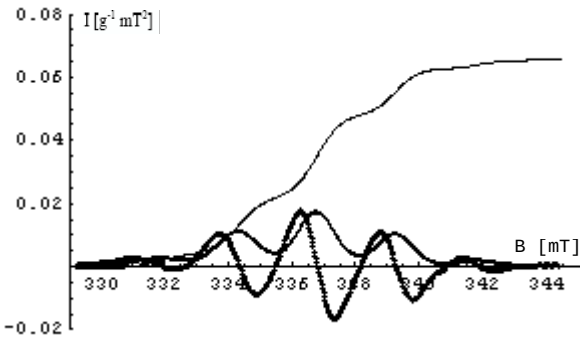

Fig20b Output spectrum (thick graph), integral resembling the absorption spectrum and double integral (thin graph) for Ala

The estimated value of the radiation chemical yield (table 16) of LiFo is higher than the value of 3.2/100eV previously cited (Vestad, 2005) but the discrepancy could be within the uncertainty.

Table 16 Double integrals and radiation chemical yield for LiFo and NaFo with Ala (as reference)

	LiFo	NaFo	Ala
I [g^{-1} mT^2]	1.08 * 10^{-7}	6.08 * 10^{-7}	1.50 * 10^{-7}
I/I_{ref} [g^{-1}]	1.39 * 10^{-5}	6.32 * 10^{-5}	1.69 * 10^{-5}
$(I/I_{ref})/D$ [g^{-1} Gy^{-1}]	1.54 * 10^{-7}	7.35 * 10^{-7}	1.78 * 10^{-7}
G [g^{-1} Gy^{-1}]	2.2 * 10^{14}	1.0 * 10^{15}	2.5 * 10^{14}
G [#/100eV]	3.5	16.5	4.0

The value for NaFo is very high but the radicals of NaFo are not stable (as reported below) and thus the absolute value is of little value. However, the result indicates a high initial radical yield which should be subject of further investigation.

4.6 RADICAL STABILITY

During each series of measurement, the signal seemed to fade rapidly, typically over 5% per hour. However, when a new series of measurements was started the signal had retained its original value or at least only faded slightly. During long series of

measurement and/or measurement at high microwave power, the cavity temperature was found to increase with over 10 K which according to Eq17 would lead to 3-4% decrease in the signal. The temperature dependence of the relaxation times might also have influenced the result but no attempt was made to estimate this effect. The problem was practically solved by cooling the cavity with liquid nitrogen with a flow adjusted to keep the cavity at room temperature. By performing this temperature control the stability of the signal could be considerably improved.

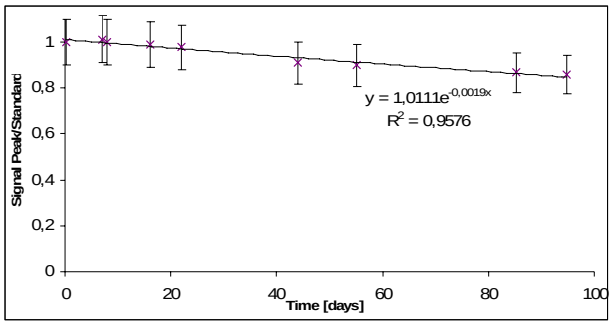

Fig21a Three month fading of ESR-signal for LiFo, normalised to Mn^{2+}(MgO) and the initial value.

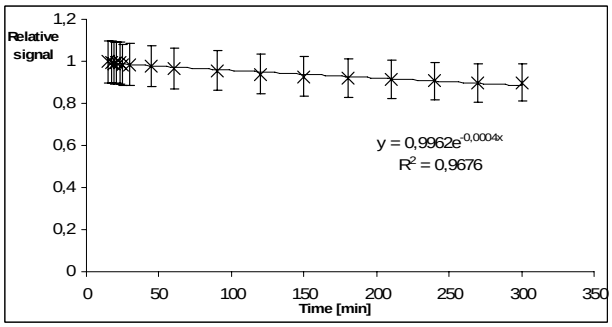

Fig21b Five hour fading of ESR-signal for NaFo, normalised to Mn^{2+}(MgO) and the initial value.

No statistically significant change in the signal of LiFo was observed during the first hours of measurement after irradiation. On the long term, the signal proved to fade exponentially (fig 21a). Extrapolation of the exponential fit yields a half life of about one year.

In comparison to LiFo, NaFo is found to fade quickly (fig 21b). Extrapolation of the exponential fit yields a half life of 30 hours. This rapid fading might be a result of radical recombination with bound water due to hygroscopic behaviour. NaFo has in fact been stated to absorb moisture from air (Mallinckrodt Baker 2006). Thus, better results might be obtained with a hygrophobic binder.

5. CONCLUSION

The reviewed methods have been successfully used for evaluation of six salts of formic and lactic acid. Lithium formate has been shown to be a good candidate for more sensitive measurements relative to the state of the art dosimeter of Alanine. Using optimal readout parameters lithium formate has been shown to be nine times as sensitive but even at moderate settings lithium formate is more sensitive. The results for lithium formate are in accordance to those of previous studies (Lund et al 2002 and Vestad et al 2003). The signal intensity of sodium formate has also proved to be high but unfortunately the signal fades rapidly.

Two modified or new methods are proposed as synthesis of the reviewed methods. The filtering method with dynamic filter limits was found to be more flexible than the previous static of Ruckerbauer et al (1996). The method was shown to be both effective and objective. However, for spectral peaks that are not narrow enough compared to interfering signals or the spectral scan width the method was found to distort the spectrum and the conventional method of baseline correction showed better results. Fortunately the impact of this distortion on the sensitivity was only a few percent. The method could probably be refined by iterative technique similar to that of Sharpe et al (1996). Use of a combination of fourier filtering, baseline correction and subtraction of empty tube and zero dose sample, as outlined by Hayes et al (2000), should also be considered.

The dose response measurement by linear regression of the entire spectrum was successful in separating the spectral peaks of the induced radicals from the background signal. Acceptable results were achieved with as few as 6 spectra and an excellent result for Lithium formate was obtained with 45 spectra at 9 different doses. Preliminary results indicate that the same method could also be used to separate the background signal of the dosimeter material from that of the test tube and spectrometer. The sensitivity derived from the dose response method is in agreement with the results from conventional linear regression to the peak height.

6. REFERENCES

AHLERS FJ, SCHNEIDER CCJ: Alanine ESR Dosimetry: An assessment of peak-to-peak evaluation. Radiation Protection Dosimetry. 37,117-122, 1991

ALM-CARLSSON G: Absorbed Dose Equations. On the derivation of a general absorbed dose equation and equations valid for different kinds of radiation equilibrium. Radiation Research, 85(2), 219-237, 1981a

ALM-CARLSSON G: Kavitetsteori - Allmänna grunder. Internal Report 43. Linköping University: Division of Radiation Physics. 1981b

ANTON M: Development of a secondary standard for the absorbed dose to water based on the alanine EPR dosimetry system. Applied Radiation and Isotopes. 62, 779-795, 2005.

ARBER JM and SHARPE PHG: Fading charcteristics of irradiated alanine pellets: The importance of pre-irradiated conditioning. Applied Radiation and Isotopes. 44, 19-22, 1993.

ARNDT R: Analytical line shapes for Lorentzian signals broadened by modulation. Journal of Applied Physics 36(8), 2522-2524, 1965.

BAGGULEY DMS, BLEANEY B, GRIFFITHS JHE, PENROSE RP and PLUMPTON BI: Paramagnetic resonance in salts of the iron group - A preliminary survey:
I. Theoretical discussion. Proceedings of the Physical Society. 61, 542-550, 1948.

BALES BL, PERIC M and LAMY-FREUND MT: Contributions to the Gaussian line broadening of the proxyl spin probe EPR spectrum due to magnetic-field modulation and unresolved proton hyperfine structure. Journal of Magnetic Resonance 132, 279-286, 1998.

BARR D, JIANG JJ and WEBER R: Performing double integrations using WIN-EPR. Bruker biospin report [cited 2004 Dec 11]. Available from URL: http://www.bruker-biospin.com/brukerepr/pdf/doubleint.pdf , 1998

BARTOLOTTA A, FATTIBENE P, ONORI S, PANTALONI M and PETETTI E: Sources of uncertainty in therapy level alanine dosimetry. Applied Radiation and Isotopes. 44, 13-17, 1993.

BERGER MJ, COURSEY JS, ZUCKER MA and CHANG J. ESTAR: Stopping-power and range Tables for electrons. NIST Physical Reference Data [cited 2000 Feb 22]. Available from URL: http://physics.nist.gov/PhysRefData/Star , 1998

BERGSTRAND ES, HOLE EO and SAGSTUEN E: A simple method for estimating dose uncertainty in ESR/alanine dosimetry. Applied Radiation and Isotopes. 49, 845-854, 1998.

BERGSTRAND ES, SHORTT KR, ROSS CK and HOLE EO: An investigation of the photon energy dependence of the EPR alanine dosimetry system. Physics in Medicine and Biology. 48, 1753-1771, 2003.

BLEANEY B, PENROSE RP and PLUMPTON BI: Paramagnetic resonance in the copper tutton salts. Journal Proceedings of the Royal Society of London A. 198(1054), 406-428, 1949.

BLOCH F: Nuclear induction. Physical Review. 70, 460-474, 1946.

BLOEMBERGEN N, PURCELL EM and POUND RV: Relaxation effects in nuclear magnetic resonance absorption. Physical Review. 73, 679-712, 1948.

BRADSHAW WW, CADENA DG, CRAWFORD GW Jr and SPETZLER HAW: The use of alanine as a solid dosimeter. Radiation Research. 17(1), 11-21, 1962.

BROTIKOVSKII OI, ZHIDOMOMIROV GM, KAZANSKII VB, SHELIMOVL BN: Modulation effects in the saturation of nonuniformly broadened ESR lines. Theoretical and Experimental Chemistry. 7(2), 206-208, 1973.

Bruker BioSpin: EPR Continuous wave practice. Bruker BioSpin GmbH [cited 2003 Dec 11]. Available from URL: http://www.bruker-biospin.com/cwpractice.html , 1999

BURLIN TE: A general theory of cavity ionization. The British Journal of Radiology. 39, 727-734, 1966.

CASTNER TG: Saturation of the paramagnetic resonance of a V center. Physical Review. 115(6), 1506-1515, 1959

CASTRO F, PONTE F; PEREIRA L: Development of physical and numerical techniques of Alanine/EPR dosimetry in radiotherapy. Radiation Protection Dosimetry. 122(1–4), 509–512, 2006

CHEN F, GRAEFF CFO and BAFFA O: Preliminary evaluation of second harmonic direct detection scheme for low-dose range in alanine/EPR dosimetry. Physics in Medicine and Biology. 47, 1357-1367, 2002.

CIESIELSKI B, SCHULTKA K, PENKOWSKI M and SAGSTUEN E: EPR study of light illumination effects on radicals in gamma-irradiated L-alanine. Spectrochimica Acta Part A 60, 1327-1333, 2004.

CIESIELSKI B, KARASZEWSKA A, PENKOWSKI M, SCHULTKA K, JUNCZEWSKA M, and NOWAK R: Reconstruction of doses absorbed by radiotherapy patients by means of EPR dosimetry in tooth enamel. Radiation Measurements. Accepted manuscript available from: doi:10.1016/j.radmeas.2007.07.013, 2007

DANILCZUK M, GUSTAFSSON H, SASTRY MD and LUND E: Development of nickel-doped lithium formate as potential EPR dosimeter for low dose determination. Spectrochimica Acta Part A. 67, 1370–1373, 2007

DE ANGELIS C, ONORI S, PETETTI E, PIERMATTEI A and AZARIO L: Alanine/EPR dosimetry in brachytherapy. Physics in Medicine and Biology. 44, 1181-1191, 1999.

DENG Y, HE G, PETRYAKOV S, KUPPUSAMY P and ZWEIER JL:Fast EPR imaging at 300MHz using spinning magnetic field gradients. Journal of Magnetic Resonance. 168, 220–227, 2004.

DOLO JM and FEAUGAS V: Analysis of parameters that influence the amplitude of the ESR/alanine signal after irradiation. Applied Radiation and Isotopes. 62, 273-279, 2005.

DOLO JM and MOIGNAU F: Use of the entire spectrum of irradiated alanine for dosimetry. Applied Radiation and Isotopes. 62, 281-285, 2005.

FAINSTEIN C, WINKLER E, SARAVI M: ESR/Alanine γ-dosimetry in the 10-30 Gy range. Applied Radiation and Isotopes. 52, 1195-1196, 2000.

FRUJINOIU C: Reconsideration of the backscatter components in the intermediate cavity theory for photon beams. Physics in Medicine and Biology. 46, 1205–1217, 2001

GALLAY R and VAN DER KLINK JJ: Resonator and coupling structure for spin-echo ESR. Journal of Physics E: Scientific Instruments, 19, 226-230, 1986.

GALLAY R and VAN DER KLINK JJ: Comment on signal power calculation in electron spin resonance. Journal of Physics E: Scientific Instruments, 20, 927, 1987.

GALLEZ B and SWARTZ HM: In vivo EPR: when, how and why? NMR in Biomedicine 17, 223-225, 2004.

GANCHEVA V, SAGSTUEN E, YORDANOV ND: Study on the EPR/dosimetry propertes of some substituted alanines. Radiation Physics and Chemistry. 75, 329-335, 2006.

GANCHEVA V, .YORDANOV ND, CALLENS F, VANHAELEWYN G, RAFFI J, BORTOLIN E, ONORI E, MALINEN E, SAGSTUEN E, FABISIAK S; PEIMEL-STUGLIK Z: An international intercomparison on “self-calibrated” alanine EPR dosimeters, Radiation Physics and Chemistry. Accepted manuscript available from: doi:10.1016/j.radphyschem.2007.06.004, 2007

GOLDBERG IB and CROWE HR: Effect of cavity loading on analytical electron spin resonance spectrometry. Analytical Chemistry 49(9), 1353-1357, 1977.

GRAY LH: An ionization method for the absolute measurement of γ-ray energy. Proceedings of the Royal Society of London A. 156(889), 578-596, 1936.

GRÜN R: Reproducibility measurements for ESR signal intensity and dose determination: High precision but doubtful accuracy. Radiation Measurements. 29, 177-193, 1998

GUSTAFSSON H, DANILCZUK M, SASTRY MD, LUND A and LUND E: Enhanced sensitivity of lithium dithionates doped with rhodium and nickel for EPR dosimetry. Spectrochimica Acta Part A. 62, 614–620, 2005

HASSAN GM, IKEYA M and TOYODA S: Lithium lactate as an ESR dosimeter. Applied Radiation and isotopes. 49, 823-828, 1998.

HASSAN GM and IKEYA M: Metal ion-organic compound for high sensitive ESR dosimetry. Applied Radiation and isotopes. 52, 1247-1254, 2000.

HASSAN GM and IKEYA M: New ESR dosimeter materials using lithium organic acid salts. Advances in ESR Applications. 18, 239-248, 2002.

HAYES RB, HASKELL EH, WIESER A, ROMANYUKHA AA HARDY BL BARRUS JK: Assessment of an alanine EPR dosimetry technique with enhanced precision and accuracy. Nuclear Instruments and Methods in Physics Research A. 440, 453-461, 2000

HEYDARI MZ, MALINEN E, HOLE EO and SAGSTUEN E: Alanine radicals. 2. The composite polycrystalline alanine EPR spectrum studied by ENDOR, Thermal annealing, and spectrum simulations. The Journal of Chemical Physics. 106, 8971-8977, 2002.

HORAN PK, TAYLOR WD, STROTHER GK and SNIPES W: Stability of radiation-induced organic free radicals: Decay by heat. Biophysical Journal. 8, 164-174, 1968

HUBBELL JH, SELTZER SM: Tables of x-ray mass attenuation coefficients and mass energy-absorption coefficients [cited 2000 Feb 22]. Available from URL: http://physics.nist.gov/PhysRefData/XrayMassCoef/cover.html , 1996

IKEYA M, HASSAN GM, SASAOKA H, KINOSHITA Y, TAKAKI S, YAMANAKA C: Strategy for finding new materials for ESR dosimeters. Applied Radiation and Isotopes. 52, 1209-1215, 2000

ISO/ASTM Internantional: Practice for use of an alanine-EPR dosimetry system. International Standard. ISO Store. ISO/ASTM 51607:2004(E). 2004

IVANNIKOV AI, TROMPER F, GAILLARD-LECANU E, SKVORTSOV VG, STEPANENKO VF: Optimisation of recording conditions for the electron paramagnetic resonance signal used in dental enamel dosimetry. Radiation Protection Dosimetry. 101(1–4), 531–538, 2002

JESCHENKE G: Introduction to magnetic resonance spectroscopy [cited 2006 May 12]. Available from URL: http://www.mpip-mainz.mpg.de/~jeschke/lect2.pdf , 2003

JIANG JJ: How to optimize EPR parameters for spin adducts. Bruker Biospin Report [cited 2004 Dec 11]. Available from URL: http://www.bruker-biospin.com/brukerepr/pdf/optimizeparameters.pdf , 1998

JUNCHENG G and ZAIYONG W: The extension of the range of NIM alanine/ESR dosimetric system to therapy level. Applied Radiation and Isotopes. 47, 1193-1196, 1996.

LARMOR J: The influence of a magnetic field on radiation frequency. Journal Proceedings of the Royal Society of London. 60, 514-515, 1897.

LEWIS GN: The atom and the molecule. Journal of the American Chemical Society. 38, 762-786, 1916.

LODGE O: The influence of a magnetic field on radiation frequency. Journal Proceedings of the Royal Society of London. 60, 513-514, 1897.

LOEVINGER R: The dosimetry of beta sources in tissue; the point-source function. Radiology. 66(1), 55-62, 1956.

LUND A, OLSSON S, BONORA M, LUND E and GUSTAFSSON H: New materials for ESR dosimetry. Spectrochimica Acta Part A, 58(6), 1301-1311, 2002.

LUND E, GUSTAFSSON H, DANILCZUK M, SASTRY MD and LUND A: Compounds of ^{6}Li and natural Li for EPR dosimetry in photon/neutron mixed radiation fields. Spectrochimica Acta Part A, 60(6), 1319-1326, 2004.

LUND E, GUSTAFSSON H, DANILCZUK M, SASTRY MD LUND A, VESTAD TA, MALINEN E, HOLE EO and SAGSTUEN E: Formates and dithionates: sensitive EPR-dosimeter materials for radiation therapy. Applied Radiation and Isotopes. 62, 317-324, 2005.

LURIE DJ: Free radical imaging. The British Journal of Radiology 74, 782-784, 2001.

LYONS RG: The difference in integrating. Radiation Measurements. 27, 345-350, 1997.

LYONS RG and TAN SM: Differentials or integrals: pluses and minuses in their application to additive dose techniques. Applied Radiation and Isotopes. 52, 1051-1057, 2000.

MAIER D and SCHMALBEIN D: A dedicated EPR analyzer for dosimetry. Applied Radiation and Isotopes. 44, 345-350, 1993.

MALINEN E, HEYDARI MZ, SAGSTUEN E and HOLE EO: Alanine radicals, Part 3: Properties of the components contributing to the EPR spectrum of x-irradiated alanine dosimeters. Radiation Research. 159, 23-32, 2003a.

MALINEN E, HULT EA HOLE EO and SAGSTUEN E: Alanine radicals, part 4: Relative amounts of radical species in alanine dosimeters after exposure to 6–19 MeV electrons and 10 kV–15 MV photons. Radiation Research. 159, 149–153, 2003.

MALINEN E, VESTAD TA, HULT EA, HOLE EO and SAGSTUEN E: Estimation of x-ray beam quality by electron paramagnetic resonance (EPR) spectroscopy. Applied Radiation and Isotopes 60, 929-937, 2004.

MALINEN E, WALDELAND E, HULT EA, HOLE EO and SAGSTUEN E: LET effects following neutron irradiation of lithium formate EPR dosimeters. Spectrochimica Acta Part A. 63, 861-869, 2006.

MALINEN E, WALDELAND E, HOLE EO and SAGSTUEN E: The energy dependence of lithium formate EPR dosimeters for clinical electron beams. Physics in Medicine and Biology. 52, 4361–4369, 2007.

Mallinckrodt Baker Inc.: Material safety data sheet sodium formate [cited 2006 Nov 07]. Available from URL: http://www.jtbaker.com/msds/englishhtml/s3770.htm , 1998

MARUANI J: Continuous Saturation of "Dispersion" Singularities and Application to Molecular Triplet States. Journal of Magnetic Resonance 7, 207-218, 1972.

MCLAUGHLIN WL: ESR dosimetry. Radiation Protection Dosimetry. 47, 255-262, 1993.

MEHTA K and GIRZIKOWSKY R: Alanine-ESR dosimetry for radiotherapy IAEA experience. Applied Radiation and Isotopes 47, 1189-1191, 1996.

NAGY V: Accuracy considerations in EPR dosimetry. Applied Radiation and Isotopes. 52, 1039-1050, 2000a.

NAGY V, PUHL JM and DESROSIERS MF: Advancements in accuracy of the alanine dosimetry system. Part 2. The influence of the irradiation temperature. Radiation Physics and Chemistry. 57, 1-9, 2000b.

NAGY V, SLEPTCHONOK OF, DESROSIERS MF, WEBER RT and HEISS AH: Advancements in accuracy of the alanine dosimetry system. Part III. Usefulness of an adjacent reference sample. Radiation Physics and Chemistry. 59, 429-441, 2000c.

NAGY V, SHOLOM SV, CHUMAK VV and DESROSIERS MF: Uncertainties in alanine dosimetry in the therapeutic dose range. Applied Radiation and Isotopes. 56, 917-929, 2002.

OLIVERO JJ and LONGBOTHUM RL: Empirical fits to the Voigt line width: A brief review. Journal of Quantitative Spectroscopy and Radiative Transfer. 17, 233-236, 1977

OLSSON SK, BAGHERIAN S, LUND E, CARLSSON GA and LUND A: Ammonium tartrate as an ESR dosimeter material. Applied Radiation and Isotopes. 50(5), 955-965, 1999

OLSSON SK, LUND E and LUND A: Development of ammonium tartrate as an ESR dosimeter material for clinical purposes. Applied Radiation and Isotopes. 52(5),1235-1241, 2000.

OLSSON S and BERGSTRAND ES: Calibration of alanine dosimeters. Internal report 92. Linköping University: Division of Radiation Physics. 2001

OLSSON S, SAGSTUEN E, BONORA M and LUND A: EPR Dosimetric properties of 2-methylalanine: EPR, ENDOR and FT-EPR investigations. Radiation Research. 157, 113-121, 2002a.

OLSSON S, BERGSTRAND ES, CARLSSON ÅK, HOLE EO and LUND E: Radiation dose measurements with alanine/agarose gel and thin alanine films around a ^{192}Ir brachytherapy source, using ESR spectroscopy. Physics in Medicine and Biology. 47, 1333-1356, 2002b.

OREAR J: Least squares when both variables have uncertainties. American Journal of Physics. 50(10), 912-916,1982

PAULI W: Uber den zusammenhang des abschlusses der elektronengruppen im atom mit der komplexstruktur der spektren. Zeitschrift für Physik, 31, 765-783, 1925.

PORTIS AM: Electronic Structure of F Centers: Saturation of the electron spin resonance. Physical Review. 91(5), 1071-1078, 1953.

PURCELL EM, TORREY HC and POUND RV: Resonance absorption by nuclear magnetic moments in a solid. Physical Review. 69(1-2), 37-38, 1946.

RABI II: Space quantization in a gyrating magnetic field. Physical Review. 51, 652-654, 1937.

REGULLA DF and DEFFNER U: Dosimetry by ESR spectroscopy of alanine. The International Journal of Applied Radiation and Isotopes. 33, 1101-1114, 1982.

REGULLA DF: Keynote lecture: ESR spectrometry: a future-oriented tool for dosimetry and dating. Applied Radiation and Isotopes. 62, 117–127, 2005.

RUCKERBAUER F, SPRUNCK M and REGULLA DF: Numerical signal treatment for optimized alanine/ESR dosimetry in the therapy-level dose range. Applied Radiation and Isotopes. 47, 1263-1268, 1996.

SAGSTUEN E, HOLE EO, HAUGEDAL SR, LUND A, EID OI and ERICKSON R: EPR and ENDOR Analysis of x-irradiated L-alanine and $NaHC_2O_4 \cdot H_2O$. Simulation of microwave power dependence of satellite lines. Nukleonika. 42, 353-372, 1997a.

SAGSTUEN E, HOLE EO, HAUGEDAL SR and NELSON WH: Alanine radicals: Structure determination by EPR and ENDOR of single crystals x-irradiated at 295 K. The Journal of Physical Chemistry. 101, 9763-9772, 1997b.

SAGSTUEN E, LUND A, ITAGAKI Y and MARUANI J: Weakly coupled proton interactions in the malonic acid radical: Single crystal ENDOR analysis and EPR simulation at microwave saturation. The Journal of Physical Chemistry A. 104, 6362-6371, 2000.

SCHAEKEN B and SCALLIET P: One year of experience with alanine dosimetry in radiotherapy. Applied Radiation and Isotopes. 47, 1177-1182, 1996.

SCHAUER DA, IWASAKI A, ROMANYUKHA AA, SWARTZ HM and ONORI, S: Electron paramagnetic resonance (EPR) in medical dosimetry. Radiation Measurements. 41, 117–123 2007.

SELTZER SM: Recent dosimetry activities at NIST. CCRI(I)/05-09 Available from URL: http://www.bipm.fr/cc/CCRI(I)/Allowed/17/CCRI(I)05-09.pdf , 2005

SHARPE PHG, RAJENDRAN K and SEPHTON JP: Progress towards an alanine/ESR therapy level reference dosimetry service at NPL. Applied Radiation and Isotopes. 47(11-12), 1171-1175, 1996.

SLEPTCHONOK OF, NAGY V and DESROSIERS MF: Advancements in accuracy of the alanine dosimetry system. Part 1. The effects of environmental humidity. Radiation Physics and Chemistry. 57, 115-133, 2000.

SMITH GW: Modulation effects in magnetic resonance: Widths and amplitudes for Lorentzian and Gaussian lines. Journal of Applied Physics. 35(4), 1217-1221, 1964.

SNIPES W and HORAN PK: Electron spin resonance studies of free radical turnover in gamma-irradiated single crystals of alanine. Radiation Research. 30(2), 307-315, 1967.

SPENCER LV, ATTIX FH: A Theory of cavity ionization. Radiation Research. 3(3), 239-254, 1955.

TRUITT JL: Spin coherence in silicon/silicon-germanium nanostructures. Dissertation submitted in partial fulfilment of the requirements for the degree of Doctor of Philosophy. Department of Physics at the University of Wisconsin-Madison [cited 2006 Okt 13]. Available from URL: http://jubjub.physics.wisc.edu/~truittj/thesis.pdf, 2004

UREÑA-NUÑEZ F, CABRAL-PRIETO A, JIMENEZ-DOMINGUEZ H, GALINDO S, BOSCH P: EPR structure of the gamma-irradiated alanine spectrum. Applied radiation and isotopes. 44(1-2), 53-57, 1993.

VESTAD TA, MALINEN E, LUND A, HOLE EO and SAGSTUEN E: EPR dosimetric properties of formates. Applied Radiation and Isotopes. 59, 181-188, 2003.

VESTAD TA, GUSTAFSSON H, LUND A, HOLE EO and SAGSTUEN E: Radiation-induced radicals in lithium formate monohydrate ($LiHCO_2 \bullet H_2O$). EPR and ENDOR studies of X-irradiated crystal and polycrystalline samples. Physical Chemistry Chemical Physics. 6, 3017-3022, 2004a.

VESTAD TA, MALINEN E, OLSEN DR HOLE EO and SAGSTUEN E: Electron paramagnetic resonance EPR dosimetry using lithium formate in radiotherapy: comparison with thermoluminescence (TL) dosimetry using lithium fluoride rods. Physics in Medicine and Biology 49, 4701-4715, 2004b.

VESTAD TA: On the development of a solid-state, low dose EPR dosimeter for radiotherpy [dissertation]. University of Oslo: Department of Physics; 2005

WAHLQUIST H: Modulation broadening of unsaturated Lorentzian lines. The Journal of Chemical Physics. 35(5), 1708-1710, 1961.

WIESER A, LETTAU C, FILL U, and REGULLA DF:The influence of non-radiation induced ESR background signal from paraffin-alanine probes for dosimetry in the radiotherapy dose range. Applied Radiation and Isotopes 44, 59-65, 1993

WIESER A, GIRZIKOWSKY R: A unique calibration curve for alanine EPR dosimetry systems. Applied Radiation and Isotopes. 47(11), 1269-1275, 1996.

YORDANOV ND and GANCHEVA V: Some new approaches in the field of solid state/EPR dosimetry. Advances in ESR Applications. 18, 227-231, 2002.

YORDANOV ND, FABISIAK S and LAGUNOV O: Effect of the shape and size of dosimeters on the response of solid state/EPR dosimetry. Radiation Measurements. 41, 257–263, 2006.

ZEEMAN O: The effect of magnetisation on the nature of light emitted by a substance. Nature [Translated by Arthur Stanton from the Proceedings of the Physical Society of Berlin]. 55, 347

ØSTERÅS BH, HOLE EO, OLSEN DR and MALINEN E: EPR dosimetry of radiotherapy photon beams in inhomogeneous media using alanine films. Physics in Medicine and Biology. 51, 6315–6328, 2006.